Tracing total and dissolved material in a western Canadian basin using quality control samples to guide the selection of fingerprinting parameters for modelling

J. P. Laceby, P. V. G. Batista, N. Taube, M. K. Kruk, C. Chung, O. Evrard, J. F. Orwin, J. G. Kerr

Tracing total and dissolved material in a western Canadian basin using quality control samples to guide the selection of fingerprinting parameters for modelling

Laceby, J.P.[a*], Batista, P.V.G.[b], Taube, N.[a], Kruk, M.K.[a], Chung, C.[a], Evrard, O.[c], Orwin, J.F.[a], Kerr, J.G.[a]

[a] Alberta Environment and Parks, 3535 Research Rd NW, Calgary, Alberta, T2L 2K8
[b] Environmental Geosciences, University of Basel, Bernoullistrasse 30, 4056 Basel, Switzerland
[c] Laboratoire des Sciences du Climat et de l'Environnement (LSCE/IPSL), CEA-CNRS-UVSQ, Université Paris-Saclay, Gif-sur-Yvette, France

*Corresponding author: J. Patrick Laceby (patrick.laceby@gov.ab.ca)

Abstract

The source dynamics of total and dissolved material in riverine systems are being affected by anthropogenic activities resulting in the degradation of waterways worldwide. Identifying the main sources of total and dissolved material is thus central to the management of increasingly scarce water resources. Here, we utilize data generated from water quality monitoring programs to investigate the sources of total and dissolved material in a large, semi-arid basin in western Canada. Our research focuses on the confluence of two major tributaries in the South Saskatchewan River Basin (SSRB) in the Province of Alberta: the Bow River (25,611 km^2) and the Oldman River (28,270 km^2). A tributary tracing technique coupled with a Deconvolutional-MixSIAR (D-MIXSIAR) modelling approach is used to estimate the potential source contributions of total and dissolved material from major tributary sites to target node sites on the main stem of the Bow River and Oldman River in addition to target nodes downstream of their confluence. In total, 812 samples were taken from 29 sites across the SSRB. A novel approach to selecting fingerprints for modelling is presented based on the analyses of additional quality control samples (146 duplicate and 172 blank samples). Overall, the Rocky Mountain headwater catchments were found to dominate the supply of material modelled using total recoverable (68%) and dissolved (76%) metals. There were seasonal fluctuations in source dynamics evident where the Bow River dominated the supply of total (69%) and dissolved (57%) material during the ice-covered season (November-March), and the Oldman River dominated the supply of total (73%) and dissolved (59%) material during the open water season (April-October). On the one hand, these seasonal dynamics are potentially the result of the extensive regulation of flow, particularly along the Bow River. On the other hand, the intensification of agriculture in the prairie/plain catchments may also facilitate the excess supply of total relative to dissolved material. For example, the Little Bow River, with ~70% agricultural land cover, contributed ~14 times more total material than anticipated based on discharge and 1.6 times more than anticipated based on unit area during the open water season. Overall, this research has improved our understanding of the source dynamics of total and dissolved material in the SSRB, providing the foundation for focussed studies targeting the main sources of total and dissolved material in this large, semi-arid basin in western Canada. In addition, our research highlights the potential of using existent data generated from water quality monitoring programs along with quality control best practices to help improve our understanding of the source dynamics of total and dissolved material in waterways around the world.

Keywords: Alberta; waterways; sediment; water resources; conservation; geochemistry

Highlights: *3 to 5 bullet points, maximum 85 characters, including spaces, per bullet point*

- The source dynamics of total and dissolved material were investigated
- Water quality monitoring data was modelled with Deconvolutional-MixSIAR
- A novel approach to select tracers based on quality control samples was presented
- Future research should examine source dynamics in reservoirs and lakes

1. Introduction

Anthropogenic activities (e.g. grazing, clearing, agriculture, and logging) have affected more than half of the Earth's terrestrial surface (Hooke et al., 2012; Richter and Mobley, 2009) impacting fundamental critical zone processes and resulting in major changes in the cycling of particulate and solute material in riverine systems (Meybeck, 2003). Elevated total and dissolved material may be indicative of the downstream transfer of contaminants transported either in the dissolved phase or bound to particulate matter (Bainbridge et al., 2012; Elbaz-Poulichet et al., 2006; Gateuille et al., 2014). Accordingly, it is important to identify and understand the source dynamics of both total and dissolved material in riverine systems in order to develop and implement best management practices that mitigate the degradation of freshwater systems (Collins et al., 2011; Gellis and Walling, 2011; Grasby et al., 1997).

Sediment source fingerprinting is a field-based technique that estimates the main sources of sediment in riverine, lacustrine and coastal systems (Douglas et al., 2003; Hatfield and Maher, 2008; Jalowska et al., 2017). This technique capitalizes on differences in physical and biogeochemical parameters between potential sources to trace sediment provenance (Klages and Hsieh, 1975; Lewin and Wolfenden, 1978; Oldfield et al., 1979). A wide variety of fingerprinting parameters have been used to investigate sediment sources (e.g. fallout radionuclides, mineral magnetic properties, major and trace element geochemistry) through being incorporated into end-member mixing models that are solved stochastically in frequentist (Collins et al., 2012; Tiecher et al., 2019; Walling et al., 1993) or Bayesian frameworks (Cooper and Krueger, 2017; Davies et al., 2018; Small et al., 2002) to apportion source contributions to target material.

Developed for stable isotope research in ecology, Bayesian mixing models such as Stable Isotope Analyses in R (SIAR) (Parnell et al., 2008) and MixSIAR (Semmens et al., 2013) are increasingly being used to model sediment sources (Boudreault et al., 2019; Garzon-Garcia et al., 2017; Koiter et al., 2013). One advantage of using these stable isotope mixing models is that they are inherently designed to include the concentration dependency of isotope ratios during end-member modelling (Mabit et al., 2018; Reiffarth et al., 2019; Upadhayay et al., 2018a). A second advantage is the relative straightforwardness of running complex Bayesian end-member mixing models in a R coding environment or with the provided graphical user interface (Stock and Semmens, 2013).

Accordingly, there has been a significant uptake of stable isotope mixing models in sediment fingerprinting research (e.g. Astorga et al., 2018; Bahadori et al., 2019; Barthod et al., 2015; Brandt et al., 2016; Bravo-Linares et al., 2018; Dutton et al., 2013; Glendell et al., 2018; Jantzi et al., 2019; Liu et al.,

2017; McCarney-Castle et al., 2017). One key innovation has been the development of functions in the R programming language that allow for the 'de-convoluted un-mixing' of sediment sources (Blake et al., 2018). Notably, the Deconvolutional-MixSIAR (D-MIXSIAR) model facilitates the downstream propagation of source contributions to sediment for multiple target sampling locations (Blake et al., 2018), which holds significant potential to generate comprehensive information on sediment source dynamics. As the development of D-MIXSIAR in the literature has predominantly focussed on small catchments (Blake et al., 2018; Upadhayay et al., 2018b), there remains a gap in our knowledge regarding the utility of D-MIXSIAR in larger catchments.

Here, we apply the D-MIXSIAR model in a large watershed in Alberta, western Canada. In particular, our research focuses on the confluence of two major tributaries in the South Saskatchewan River Basin (SSRB), the Bow River (25,611 km^2) and the Oldman River (28,270 km^2) (Figure 1). Snowmelt and precipitation runoff in the Rocky Mountain headwaters are hypothesized to drive the downstream transfer of total and dissolved material in this region. To test this hypothesis, a D-MIXSIAR modelling approach, using dissolved and total recoverable metals analyzed on surface water grab samples (n = 812) taken monthly for approximately three years (2016-2018), was run for target sampling sites on the main stem (i.e. nodes) upstream and downstream of the confluence of the Bow and Oldman Rivers. A tributary tracing technique is employed where surface water grab samples from 22 different tributaries are used as source samples that are de-convoluted with the D-MIXSIAR model through seven main stem node sites (i.e. target samples) to provide a comprehensive understanding of the source dynamics of total and dissolved material in the SSRB.

Our research design includes the sampling and analyses of 318 quality control samples. In particular, field blank samples (n = 172) estimate the potential bias (i.e. contamination) in the dataset whereas duplicate samples (n = 146) assess the variability (i.e. precision) of the potential fingerprinting parameters. Results from a comprehensive statistical analysis of the duplicate and field blank samples, based on best practices developed by the United States Geological Survey (i.e. Bender et al., 2011; Mueller et al., 2015) are used to develop a novel approach to select fingerprinting parameters to be included in end-member mixing models based on quality control samples.

The overall objective of this research is to investigate the source dynamics of total and dissolved material from tributaries in the SSRB in order to help understand and manage these waterways in the context of land use intensification and a changing climate. In particular, the modelling results may highlight tributaries that disproportionately contribute total and dissolved material, which require

targeted management. Our research also highlights a particularly powerful approach to utilize data generated from water quality monitoring programs, coupled with an appropriate quality control framework, to investigate total and dissolved material dynamics worldwide. To best of our knowledge, this is one of the first attempts to use regional water quality monitoring data, including quality control best practices, to simultaneously trace both the total and dissolved fractions with the sediment source fingerprinting technique.

2. Material and Methods

2.1 Study Site

In south eastern Alberta, Canada, the Bow (25,611 km^2) and Oldman Rivers (28,270 km^2) merge to form the South Saskatchewan River, which flows eastward towards Lake Winnipeg and discharges eventually into Hudson's Bay as part of the Nelson River basin (Figure 1). The headwaters of the Bow and Oldman Rivers are situated on the eastern side of the Continental Divide in the Rocky Mountains. These watersheds transition from alpine and foothill landscapes in their montane headwaters (maximum elevation: ~3500 m) to prairie and grassland plains as they cross the province of Alberta (minimum elevation: ~600 m). The geology of the Bow and Oldman watersheds, in their montane headwaters, is mainly calcareous limestone, dolomite and shale predominantly of Paleozoic age. The geology transitions downstream to calcareous feldspathic sandstone, siltstone, mudstone and coal beds predominantly of Cretaceous and Tertiary age in the foothills and prairie landscapes (Hamilton et al., 1999). During the last glaciation, between ~18,000 to 13,000 years before present, the Laurentide Ice Sheet retreat left behind varying thicknesses of glacio-fluvial, glacio-lacustrine, Aeolian and till deposits across the Albertan prairies (Dyke and Prest, 1987). These deposits continue to exert a strong control on the source dynamics of total and dissolved material throughout Alberta.

Land use and land cover in the study watershed, as delineated from the outlet sampling site (SSR2 - Figure 1), are dominated by agriculture (ca. 40% of the total area) followed by 21% grassland, 16% forest, 5% exposed rock, 5% water, reservoirs and wetlands, 4% shrub, 3% linear transport, 3% disturbed (including urban land covers), 1% forestry and 1% mining including oil and gas operations. Overall, land use and land cover are highly variable in the tributary source watersheds, progressing from catchments dominated by relatively natural land cover in the Rocky Mountain headwaters to agriculturally dominated watersheds in the lower reaches of the study basin. The main agricultural crops or activities in the outlet sampling site (SSR2) watershed, according to the Agriculture and Agri-food Canada, Annual Crop Inventory

(AAFC, 2018) were spring wheat (36%), canola / rapeseed (22%), barley (16%), peas (8%) and pasture / forage (6%).

The SSRB has a predominantly semi-arid climate with a mean annual precipitation of 435 mm (Kerr, 2017) and a precipitation gradient across the catchment from the Rocky Mountains headwaters (~600 mm annually) to the drier downstream prairie region (~300 mm annually) (Halliday, 2009). In most of the non-montane headwater regions, evapotranspiration exceeds precipitation (Schindler and Donahue, 2006). Although there is sufficient rainfall in the region to sustain crop production with irrigation, little to no runoff is generated from the grassland and prairie landscapes that include dead drainage areas (Godwin and Martin, 1975; Halliday, 2009). In fact, 71% of Canada's irrigated land is found in the Province of Alberta (Statistics Canada, 2017), the majority of which is in the SSRB. As such, there is an extensive regulation of rivers in this region, including 13 dams, four weirs and eight reservoirs in the Bow River watershed (AMEC, 2009) along with thee major reservoirs and more than a dozen other water control structures in the Oldman River watershed (Koning et al., 2006).

The SSRB basin is characterized by short summers and cold winters with a mean annual temperature of ~3°C (Downing and Pettapiece, 2006). This seasonal pattern results in the rivers being predominantly covered with ice during winter (November-March) followed by periods of snow-melt runoff, first from the prairies and then from the mountain snowpack (Pomeroy et al., 2005). Snowmelt and rainfall during snowmelt generates most of the annual runoff and flow (Halliday, 2009). Accordingly, the region's dominant hydrological event is the annual melting of the Rocky Mountain snowpack starting in early May and lasting for approximately 40 days (Grasby and Hutcheon, 2000). Discharge is greatest in June when the peak in montane runoff coincides with the month with the most rainfall. Although there can be significant rainfall events in May and June, the mountain snowmelt runoff generally dominates the hydrograph. For example, snowmelt from the Rocky Mountains may produce between 70-90% of the annual discharge in the Oldman River, depending on annual variation in snowpack (Byrne et al., 2006).

2.2 Sample Design

Water quality data was obtained from two Alberta Environmental and Parks (AEP) monitoring programs: the long-term river monitoring network (LTRN) and the tributary monitoring network (TMN). The LTRN program generally has monitored sites on the main stems of Alberta's major rivers for the last 30+ years. In 2016, AEP initiated the TMN program to investigate water quality dynamics in smaller tributaries across the province. Here, we capitalize on data generated by these programs, to illustrate how

171 water quality data from monitoring programs are often naturally suited to be used in tributary tracing
172 research designs (i.e. where samples from potential tributaries are incorporated into end-member mixing
173 models as potential sources) and incorporated into sediment fingerprinting research. Water quality
174 monitoring data has the potential to be particularly powerful when coupled with the D-MIXSIAR model
175 that allows for the propagation of downstream tributary site source contributions to total and dissolved
176 material through multiple main stem target sites, or nodes, in large river basins.

177 Dissolved and total recoverable metals were analyzed for one-litre grab samples of surface water
178 taken monthly in pre-cleaned, high-density polyethylene bottles at surface water quality monitoring sites
179 as part of the TMN and LTRN programs between April 2016 and December 2018 (Table 1). An illustration
180 of the timing of the sampling regime on the main stem sites plotted with discharge can be found in Figure
181 S1. In total, 812 samples were obtained, 224 during the winter ice-covered season (November – March)
182 and 588 during the open water season (April – October). For some tributary sites (n = 9), it was not possible
183 to sample during the winter. For the majority of the target site nodes, there were 21 samples obtained
184 during the open water season and 12 during the ice-covered season (Table 1). In the Bow River catchment,
185 samples were obtained at 15 sites, including three target site nodes (Figure 1). In the Oldman River
186 catchment, samples were taken at 10 sites, including two target nodes. Finally, there were four sampling
187 sites, including two nodes, in the South Saskatchewan River sub-basin downstream of the confluence of
188 the Bow and Oldman Rivers. In total, 29 sites were sampled, of which 22 were potential sources, along
189 with seven target site nodes. For the final D-MIXSIAR model, the source contributions from the 22
190 potential source sites are estimated for the outlet site of this study basin on the South Saskatchewan River
191 downstream of Medicine Hat (SSR2 – Figure 1).

192 No particle size fractionation was undertaken owing to the fact that we are comparing tributary site
193 water quality grab samples to water quality grab samples from main stem node sites with the major
194 particle size sorting effects generally occurring during sediment generation, mobilization and initial
195 transport phases which have been assumed to have already materialized (Laceby et al., 2017; Laceby et
196 al., 2015a). Additionally, to address the potential solubility of various metals (e.g. Ca, K, Mg, Sr)(Kraushaar
197 et al., 2015), which may be transported primarily in the dissolved phase (Meybeck and Helmer, 1989), D-
198 MIXSIAR models were run on both the dissolved and total recoverable metal datasets to compare
199 differences in their modelled contributions to dissolved and total material across the SSRB.

200 Twenty-nine metals were analyzed by Innotech Alberta's Environmental Analytical Laboratory in
201 Vegreville, Alberta (Table 2) for both the total recoverable fraction (i.e. the total water sample) and the

dissolved fraction which was filtered with 0.45 µm cellulose acetate filter paper. Total water samples and the dissolved filtrate were preserved in Vegreville by staff at Innotech with 1% concentrated SeaStar high purity nitric acid for at least 16 h, thereafter ~50 ml of the preserved sample was digested for 20 m at 180°C and 200 PSI. A portion of the digested solution was then introduced directly to an inductively coupled argon plasma-mass spectrometer with internal standards added online. Although Se and Cl are not metals, they will be referred to in the results and discussions as metals as they are included in the metal analysis results provided by Innotech. We use the term total material, rather than total suspended solids, as total material includes both suspended and dissolved material, which is representative of how the total recoverable metals were analyzed in our water samples. Additionally, we use the term dissolved material rather than total dissolved solids to emphasise the fact that the dissolved metals are likely representative of only a fraction of total dissolved solids (e.g. inorganic salts, nutrients, etc.). Our objective of using the term material is to indicate that modelling results are illustrative of the main sources of the bulk of the material being sampled and analyzed rather than identifying sources of individual constituents of the dissolved or total material.

2.3 Quality Control Samples

2.3.1 Blank samples

Blank samples quantify the potential positive or negative bias in environmental data resulting from contamination (Mueller et al., 1997; Riskin et al., 2018). In general, positive bias is introduced from contamination in sampling and analyses which may result in environmental data being reported at a higher level than actual levels present in the environment (Mueller et al., 2015). Here, field blank samples are used to assess the positive bias (i.e. contamination) that may result from the entire process of sample collection through sample storage and laboratory analyses. Blank water, obtained from Innotech, was used to rinse the sample containers three times prior to being used to fill these containers with a field blank water sample for analyses. In total, 172 field blank samples were collected by staff at the Calgary field office during the sampling period.

The frequency and magnitude of potential contamination in the field blank samples is directly related to 2,015 similar one-litre grab samples of surface water collected by AEP's Calgary field office from January 2016 to December 2018. After Mueller et al. (2015), the 90 percent upper confidence limit (UCL) for the 95th percentile concentration of the field blank dataset, is representative of the maximum contamination anticipated, with a 90% confidence, in 95% of the sample population. Accordingly, this provides 90%

confidence that this contamination level would not be exceeded in more than 5% of the sample population, including both the environmental and field blank datasets. Following Mueller et al. (2015), a binomial function calculates a distribution-free UCL for the field blank percentiles, ranks the data in ascending order, and then uses a binominal probability function (*B)* to calculate the UCL with equation 1:

$$B(p, n, U-1) \geq 1-\alpha \quad \text{(Eq. 1)}$$

Where *p* is the percentile/100, n is the number of samples, *U* is the rank, and α is the significance level of the confidence interval. The 100(1-α)-percent UCL for the (100)pth percentile of potential extraneous contamination in the population is estimated by the analytical value of a given parameter at rank *U* in a set of *n* field blanks. As an example, for 100 field blank samples, the UCL (90%) at the 95th percentile, hereafter referred to as the B95-90 value, is:

$$B(0.95, 100, U-1) \geq 0.90 \quad \text{(Eq. 2)}$$

Solving for U yields U=99; therefore, the B95-90 value is the analytical result for the 99th ranked blank sample.

An example of this statistical procedure is outlined in more detail in Mueller et al. (2015) and a comprehensive report on field blank analyses for samples taken across the province of Alberta is presented in Laceby et al. (in press). The difference between the environmental data and the B95-90 value is used to calculate the potential for environmental contamination based on relating the percent of field blanks above the detection limit and the amount of environmental data within one order of magnitude of the B95-90 value with this procedure again outlined comprehensively in both Mueller et al. (2015) and Laceby et al. (in press).

2.3.2 Duplicate samples

Duplicate samples are used to estimate random error in environmental data potentially generated during sample collection, storage and laboratory analyses (Mueller et al., 2015; Riskin et al., 2018). In particular, duplicate samples assess the overall variability (i.e. precision) of environmental monitoring programs, whereas field blank samples investigate the potential bias (i.e. accuracy). During our study period, 146 duplicate samples were collected by the Calgary field office. The majority of duplicate samples were collected concurrently (i.e. simultaneously within 1 m distance), with some duplicates obtained sequentially (i.e. within 2 minutes and 1 m distance) in limited instances owing to logistical constraints. Prior to sampling, duplicate bottles were rinsed three times with river water.

The variability in analyte detection and the variability relative to environmental data were both determined from the duplicate sample analyses. Variability in analyte detection is calculated by first determining the percent of duplicate sets with inconsistent detections (i.e. duplicate sets that contain both a non-detect and a detected value) (Mueller et al., 2015). Second, the number of duplicate sets with inconsistent detections is divided by the total amount of duplicate sets minus the number of pairs with consistent non-detects (i.e. two MDLs). Following Mueller et al. (2015), a one-sided UCL is calculated for the percentage of inconsistent duplicate sets with equation 3:

$$P_U = 100\left\{1 + \frac{n - x}{(x+1)F_{1-\alpha,df_1,df_1}}\right\}^{-1} \quad \text{(Eq. 3)}$$

where P_U is the UCL (%), n is the total number of duplicate pairs, x is the number of duplicate pairs having inconsistent detects, and F is a percentage point derived from the F distribution for a 100(1-α) percent confidence with the degrees of freedom being: $df_1 = 2x + 2$ and $df_2 = 2n - 2x$ (Mueller et al., 2015).

To relate duplicate variability to the environmental data, the variability in analyte concentrations is evaluated. Here, we use a bias-corrected log-log regression model, which is based on the approximate linear relationship in the logarithms of the duplicate mean and standard deviation concentrations, to evaluate duplicate variability across their concentration range (Mueller et al., 2015). For a comprehensive discussion on the suitability of this approach to analyze duplicate samples and detailed examples, see Mueller et al. (2015). The regression model is based on equation 4:

$$\log(SD) = B_0 + B_1 \log(C) \quad \text{(Eq. 4)}$$

where log(*SD)* is the logarithm of the standard deviation (SD) of the paired duplicate sample concentrations, B_0 is the y-axis intercept of the regression line, which is estimated by the least squares method, B_1 is the regression line slope, and log(*C*) is the logarithm of the mean of the paired duplicate concentrations.

The residuals from this regression equation are then back-transformed to their original scaling. The mean of these residuals is included in equation 5 as a bias correction factor (BCF) to compensate for transformation bias when the SD is calculated in original units (e.g. mg/L):

$$SD = BCF\left\{10^{[B_0 + B_1 log(C)]}\right\} \quad \text{(Eq. 5)}$$

Equation 5 is then used to determine duplicate variability as the mean bias-corrected SD for any given parameter concentration, C (Mueller et al., 2015).

To relate the variability in the duplicate samples to the environmental data, we estimate the uncertainty of analyte values measured in environmental samples through constructing confidence intervals for environmental sample concentrations with equation 6 (Mueller et al., 2015):

$$[C_L, C_U\,] = C \pm Z_{(1-\alpha/2)^\sigma} \quad \text{(Eq. 6)}$$

where C is the measured environmental analyte value, C_L and C_U are the lower and upper confidence limits (CL) of the analyte value for the 100(1-α/2) confidence interval percent, *Z* is the percentage point of a normal standard curve containing an area of 100(1-α/2) percent, α represents the probability of the confidence interval not including the true analyte value (i.e. α is 0.9 for the 90% CL), and σ is the SD of the analyte value calculated with equation 5. To contextualize this duplicate analysis, we calculate the mean confidence interval (M-CI), which is the average C_L and C_U when applying equation 6 to each percentile of the environmental data (n = 2,015). Of note, both the duplicate and blank analyses include all LTRN and TMN samples taken by the Calgary field office, including several sites not included as nodes or tributary source sites in this fingerprinting research in order to comprehensively quantify the overall potential bias and contamination of samples obtained during the study period as a larger sample size should theoretically result in improved estimates of potential bias and variability.

2.4 Source Fingerprinting

The results from the quality control analyses were used to remove metals that have a high potential for bias (i.e. contamination) or variability. First, metals were removed if they had a potential for contamination greater than 20% based on the field blank analyses. Second, metals were removed that had an upper confidence limit for inconsistent detection greater than 20% and/or a duplicate variability (i.e. M-CI) across the concentration range greater than 20%. The 20% upper limit of bias and variability was selected because it is the maximum acceptable relative percent difference between laboratory duplicates and the maximum allowable bias on laboratory spike samples, which if exceeded, the batch of samples requires reanalysis. After removing metals based on the quality control analyses, a mean and standard deviation (SD) conservative bracket/range test (e.g. the mean of the target material falls within one SD of the source tributary material) was used to select metals for modelling. A separate bracket/range test was conducted for each individual MixSIAR model. Owing to MixSIAR's capacity to handle correlated data, no further tracer selection steps were included following the work of Smith et al. (2018).

The D-MIXSIAR model was run in the R-programming Language using MixSIAR as the model engine based on code published as supplementary information in Blake et al. (2018) with MixSIAR's mathematical

formulation outlined in Stock et al. (2018). All models were run first with normal distributions as Smith et al. (2018) illustrated that the removal of tracers with non-normal distributions may reduce the overall accuracy of MixSIAR results. Additionally, we applied log-normal, square root and cube root transformations to our source data in very-short and very long MixSIAR model runs to investigate the sensitivity of MixSIAR to assumptions around the normality of source data, which was assessed after the transformations, or the lack there of for normal distributions, with Shaprio-Wilks tests.

The NADA package in R implemented regression on order statistics (ROS) to estimate the mean and standard deviation of the source metal concentrations with censored data (e.g. below minimum detection limits) to generate the normal distributions that were modelled with MixSIAR. In total, there were seven data points in the dissolved modelled data that were below detection limits whereas there was no censored data in the total recoverable modelled data.

MixSIAR was run with the residual error model structure, an uninformative prior, all Dirichlet hyperparameters set to one, and the Markov Chain Monte Carlo (MCMC) set to a very long chain length of 1,000,000, with a burn in of 700,000, and a thinning of 300 for three chains (following Blake et al., 2018). Additionally, a very short chain length of 10,000 with a burn in of 5,000 and a thinning of 5 for three chains was used to investigate the impact of the source distributions. The Gelman-Rubin diagnostic was used to assess model convergence and none of the variables modelled had a Gelman-Rubin diagnostic > 1.01 with the very long run times.

Owing to the strong seasonal influence on hydrological dynamics in the region, we ran three model scenarios. First, all annual data was modelled. Second, we ran models for the open water season (April to October). Third, we ran models for the ice-covered season (November to March). In summary, the D-MIXSIAR framework de-convolutes the posterior proportion contributions sequentially for each node progressing downstream while propagating the uncertainty through estimating full posterior distributions for the model results for each potential source (Blake et al., 2018). All analyses, modelling and plotting of results for this manuscript were conducted in the R programming language (R Development Core Team, 2011) with multiple packages (i.e. devtools, ggplot2, R2jags, RGtk2, ggord, data.table, tidyverse, Hmisc, matrixStats, MASS, klaR, reshape2, psych, foreach, Rsolnp, MixSIAR, rjags, NADA, tidyhydat, cowplot, plyr, stringr, tibble, scales, gridExtra, egg, forcats, tidyhydat and dplyr).

3. Results

3.1 Fingerprint Selection for modelling

For the 29 total recoverable metals analyzed, including Cl and Se, only 12 passed the quality control screening. From the field blank analysis, there were four metals with a potential for environmental contamination greater than 20% (Cl, Cu, Pb, and Zn - Table 2). Regarding the duplicate analyses, only Bi had a greater than 20% UCL in inconsistent detections. In addition, 14 metals had an M-CI greater than ±20% (Ag, Al, Be, Bi, Cd, Co, Cr, Ni, Pb, Th, Tl, Se, Sn and Zn) including four metals with an M-CI greater than ±50% (Ag, Bi, Cd, and Sn). Overall, the quality control screening removed 59% of the metals analysed with 12 (41%) moving on to the bracket/range test (As, B, Ba, Ca, Fe, Li, Mn, Mo, Sb, Sr, U and V). Between five and 12 total recoverable metals were selected for modelling the three scenarios (i.e. ice, open & all samples) for each target node based on the conservative bracket/range test requiring the mean node concentrations to plot within one standard deviation of source concentrations (Table 3). Box plots of all total recoverable metals modelled are provided in the supplementary information (Figures S2 to S13).

For the 29 dissolved metals analyzed, including Cl and Se, only 11 passed the quality control screening. Regarding the field blank analysis, there were three metals with a potential for environmental contamination greater than 20% (Al, Cu, and Ti - Table 4). Regarding the duplicate analyses, five metals had a greater than 20% UCL in inconsistent detections (Ag, Be, Bi, Cr and Pb). In addition, 15 metals had an M-CI greater than ±20% (Ag, Al, Bi, Cd, Co, Cr, Fe, Ni, Mn, Pb, Th, Tl, Se, Sn and Zn) including four metals with an M-CI greater than ±50% (Ag, Pb, Th and Sn) and one that was greater than 100% (Cr). Overall, the quality control screening removed 62% of the dissolved metals analysed with 11 (38%) moving on to the bracket/range test (As, B, Ba, Ca, Cl, Li, Mo, Sb, Sr, U and V). Between four and 11 dissolved metals were selected for modelling the three scenarios (i.e. ice, open & all annual samples) with the conservative bracket/range (Table 3). Box plots of all dissolved metals modelled are provided in the supplementary information (Figures S14 to S24).

3.2 Total Verses Dissolved Metals

On average, 64% (SD 30%) of the total recoverable metals were dissolved material. For the total recoverable metals selected for modelling, this increased to 76% (SD 33%). There were only three modelled metals with a dissolved to total recoverable ratio below 50% (Fe: 8%, Mn: 16% and V: 49%), whereas the other total recoverable metals modelled were predominantly compromised of dissolved material (i.e. >80%) (Table 5). The dominance of dissolved material in the modelled dataset was evident for the majority of TSS concentrations (TSS <50 mg: Mean (M) 78%, SD 33%, TSS between 50-100mg: M 70%, SD 37%, and TSS between 100-1000 mg/L: M 59%, SD 37%). The dissolved fraction constituted the minority of material for TSS concentrations >1000 mg/L, where it only comprised a mean of 38% (SD 36%)

of the metal concentrations modelled, although there were only 4 samples with TSS concentrations > 1000 mg/L. The metal concentrations in the one litre water grab samples are thus predominantly comprised of dissolved material.

Accordingly, the modelled source contributions with total recoverable and dissolved metals should theoretically be similar as the majority of the material is dissolved. Any deviations between the modelled source contributions with the total recoverable and dissolved metals should highlight differences between the source dynamics of total and dissolved material across the SSRB. For example, in situations where sites have relatively similar modelled source contributions with both total recoverable and dissolved metals, it can be assumed that model results from both of these metals datasets are representative of the dissolved fraction. In contrast, for situations where model results from the total recoverable metals data are greater than those estimated with dissolved metals, the source contributions modelled using the total recoverable metals are likely to be representative of suspended material (e.g. particulate matter, sediment, etc.).

3.3 MixSIAR Sensitivity to Source Data Transformations

Overall, 834 and 821 respective total recoverable and dissolved metal source distributions were incorporated into MixSIAR when modelling the ice-covered (n 265, 300), open water (n 277, 259), and all annual samples (n 279, 275). A log-10 transformation achieved the greatest degree of normality in the source dataset with a mean (M) of 61% (SD 3%) for dissolved metals (DM) and 56% (SD 0.2%) for total recoverable metals (TRM) when including the ice-covered, open water and all annual source distributions, followed by the cube root (DM: 55% SD 2.1%; TRM: 47% SD 0.8%) and square root transformations (DM: 54%, SD 0.9%; TRM: 43%, SD 0.8%). In the absence of any transformation, the source distributions of 48% (SD 0.3%) of the dissolved metals and 37% (SD 0.2%) of the total recoverable metals were distributed normally. Transformations to the source data prior to modelling with D-MIXSIAR had little to no impact on source apportionment results with a very long run time. The average standard deviation for all source contributions for all models (i.e. ice, open and all annual samples) with normal, log-normal and square root and cube root transformations was only 0.1% when modelling with a very long run time. In fact, the maximum standard deviation for modelled source contributions to target material was only 0.8%, indicating that the nature of the source data had limited impact on the model outputs with the very long run times. In contrast, the transformations resulted in a significantly higher standard deviation in results for models with very short run times (paired t-test results: $t = -6.041$, $df = 131$, p-value = <0.001), which had an average standard deviation of 0.7% and a maximum standard deviation of 7.8%. Accordingly, the

results presented below are from models with very-long run times and the conventional normal distributions, although any of the four approaches to the source data would provide nearly identical results using dissolved and total recoverable metals data modelled with very long run times.

3.5 D-MIXSIAR model results

For the D-MIXSIAR model run using the dissolved metals dataset, the Bow River headwaters were estimated to contribute the most material (M 31%, SD 6%) for all annual samples followed by Belly River (M 15%, SD 5%) and the Oldman River headwaters (M 14%, SD 4-5%) (Table 6). Although the Belly River's modelled contributions using the dissolved metals data were relatively stable over the ice-covered and open water seasons (M ~15%), the Bow River headwaters modelled contribution decreased from 29% (SD 7%) in the ice-covered season to 22% (SD 8%) in the open water season. In contrast, the Oldman River headwaters contribution, modelled using the dissolved metals, increased from 10% (SD 5%) during the ice-covered season to 21% (SD 7%) during the open-water season. The Little Bow River (M 7%, SD 3% for annual samples), the only other catchment with a noteworthy source contribution >5%, modelled using the dissolved metals, fluctuated from a 2% (SD 2%) contribution during the ice-covered season to 9% (SD 4%) during the open water season. As anticipated, seasonal fluctuations in the mean contribution ratios (MCRs) reflected these source contributions modelled using dissolved metals with the Belly River contributing approximately twice (MCRs between 1.94 – 2.04) as much material as anticipated based on unit area across all seasons. The Oldman River headwaters also contributed twice as much material as anticipated during the open water season (MCR 2.04) relative to essentially an expected contribution based on watershed area during the ice-covered season (MCR 1.02). The Bow River headwaters were modelled to contribute 1.78 times more material using dissolved metals than anticipated based on unit area during the ice-covered season compared to 1.38 times more during the open water season. The Little Bow River fluctuated from contributing almost 85% less than anticipated based on unit area in the ice-covered season (MCR 0.16) to only ~30% less during the open water season (MCR 0.68). Overall, the montane headwater catchments in the Bow and Oldman Rivers were modelled to contribute 77% using the dissolved metals dataset in the open water season, compared to 70% during the ice-covered season, and 76% when modelling all annual samples. This results in the montane headwaters being modelled using dissolved metals to contribute ~30% more material than anticipated in the open water season (MCR 1.30) and for all annual samples (MCR 1.29) versus ~20% more material than anticipated during the ice-covered season (MCR 1.19) based on their watershed area.

435 The modelling results using the total recoverable metals also had pronounced seasonal variations.
436 When modelling all annual samples using the total recoverable metals, the Bow River headwaters were
437 estimated to provide the most material to the SSR2 outlet node, contributing 27% (SD 8%), followed by
438 the Oldman River headwaters (M 12%, SD 5%), the Belly River (M 9%, SD 5%), the Little Bow River (M 9%,
439 SD 4%), the Saint Mary River (M 8%, SD 4%) and New West Coulee (M 7%, SD 4%) (Table 6). During the
440 ice-covered season, the Bow River headwaters were deconvoluted using the total recoverable metals to
441 contribute the most material (M 31% SD 8%), followed by the Belly River (M 9%, SD 6%), New West Coulee
442 (M 7%, SD 6%) and the Highwood River (M 7%, SD 5%). During the open water season, the Little Bow River
443 was modelled using the total recoverable metals to contribute the most material (M 20%, SD 7%),
444 followed by the Oldman River headwaters (M 18%, SD 6%), the Saint Mary River (M 14%, SD 6%), the Belly
445 River (M12%, SD 5%) and the Bow River headwaters (M 11%, SD 7%). This seasonal variation in modelled
446 source contributions is again clearly evident in the MCRs. The Bow River headwaters shift from an MCR of
447 0.69 in the open water season to 1.94 in the ice-covered season. In contrast, several catchments in the
448 OMR have major increases in their MCRs in the open water season with the Little Bow River shifting from
449 0.09 in the ice-covered season compared to 1.61 in the open water season. The Oldman headwaters
450 (OMR1) shifts from an MCR of 0.48 in the ice to 1.97 in the open season, the Saint Mary River from 0.3 in
451 the ice to 1.85 in the open season and the Belly River shifting from 1.18 in the ice to 1.5 in the open season.
452 Overall, montane headwater catchments in the Bow and Oldman Rivers were modelled using the total
453 recoverable metals to contribute 68% of the material for all annual samples compared to 64% in the open
454 water season and 62% during the ice-covered season. Accordingly, the montane headwaters were
455 modelled to contribute between 5-15% more material than anticipated based on watershed area with an
456 MCR of 1.05 for the ice-covered season, 1.08 in the open-water season and 1.15 for all annual samples.

457 Clearly, there was a major shift in the estimate of tributary contributions between the two main
458 seasons. When summing all tributary D-MIXSIAR model contributions, the Bow River was estimated to
459 contribute 57% and 69% using the dissolved and total recoverable models respectively in the ice-covered
460 season compared to 38% and 24% during the open water season. In contrast, the Oldman River's summed
461 modelled contributions increased from 34% and 22% using the dissolved and total recoverable metals
462 respectively in the ice-covered season to 59% and 73% during the open water season. This seasonal
463 variation in material modelled using total recoverable metals is predominantly driven by a 20% decrease
464 in contributions from the Bow River headwaters site in the open water season relative to the ice-covered
465 season, with multiple tributaries in the Oldman River all contributing more material in the open water
466 season relative to the ice-covered season (i.e. increases of 19% in the Little Bow River, 14% in the Oldman

River headwaters, and 11% in the Saint Mary River). The seasonal variation in source contributions modelled using dissolved metals was more muted with only a 6% decrease in contributions from the Bow River headwaters site in the open water season relative to the ice-covered season with multiple tributaries in the Oldman River basin modelled to contribute more dissolved material in the open water season relative to the ice-covered season (i.e. increase of 11% in the Oldman River headwaters, 7% in the Little Bow River and 7% in the Saint Mary River).

4. Discussion

4.1 Quality Control Analyses

As MixSIAR is not limited by a three-step selection process (e.g. bracket/range test, Kruskal-Wallis h-test, and discriminant function analyses) (Smith et al., 2018), it facilitates the development of alternative approaches to identify appropriate fingerprints to include in end-member mixing models. Accordingly, we presented a novel approach using quality control samples to guide fingerprint selection for modelling. Overall, we found that the majority of the metals (total recoverable 59%, dissolved 62%) analyzed in one-litre grab samples of surface water had a bias (i.e. blank sample contamination) and/or a variability (i.e. duplicate replicability) greater than 20%. In particular, our results highlight the fact that routinely measured metals data may not have equivalent uncertainty. As sediment mixing models advance (e.g. Cooper and Krueger, 2017; Lizaga Villuendas et al., 2018; Pulley and Collins, 2018; Sanisaca et al., 2017), ideally the quality of data (i.e. bias and variability) could be incorporated directly into mixing models in addition to the reporting of results.

Importantly, the potential for bias and variability evident in our metals data is likely present in other research programs analyzing particulate material collected with discrete, low volume grab samples of water, or potentially even automated stage samplers. Of note, the M-CI value used to select metals represents the mean confidence interval (e.g. ±20%) across all percentiles of environmental data. This mean value is masking elevated variability at lower concentrations. For example, the average M-CI for the 50^{th} percentile of dissolved and total recoverable metals that were not modelled was ±40% and ±35% respectively, whereas it was ±55% and ±53% for the 10^{th} percentile (Figure 2). In contrast, the average M-CI for dissolved and total recoverable metals that were modelled was ±6% and ±7% respectively for the 50^{th} percentile versus ±9% and ±8% for the 10^{th} percentile. Clearly the quality of the data generated for individual metals varies greatly (i.e. Figure 2) and the bias and variability of environmental data ideally should be accounted for more regularly in sediment fingerprinting research.

Whether similar levels of bias and variability are evident in soil and sediment samples (e.g. lag deposits, time integrated samplers) requires further research and analyses. The challenge with soils and sediments will likely revolve around metals with low abundances (e.g. rare earth elements / lanthanides) where the potential for bias and variability may arise in the field (e.g. sampling design and device contamination), laboratory (e.g. sieving, grinding and drying samples), and/or during analytical analyses (e.g. digestion procedures). As such, it would be beneficial for researchers to analyze replicate soil and sediment samples, along with some variant of consistent blank reference soils (e.g. Fernandez et al., 2014; Guzmán et al., 2010), to improve our understanding of the potential for variability and bias in these media. Although there will be obvious trade-offs with respect to increased analytical costs, we feel it is important for sediment fingerprinting researchers to start to entertain the notion of incorporating quality control best practices into their research design, end-member mixing models and reporting of results.

4.2 Total and Dissolved Source Dynamics

Watersheds originating in the Rocky Mountains or foothills region, with >25% of their landscapes having a slope >10%, were modelled to supply 76% of the material using dissolved metals and 68% using total recoverable metals to the outlet node (Site SSR2). The Bow River watershed was modelled to contribute more dissolved (53%) and total material (53%) than the Oldman River watershed (DS 46% and TS 44%) for all annual samples. For dissolved and total material, there was a clear shift in source contributions from these two major river systems during the ice-covered and open water seasons. During the ice season, the Bow River supplied the majority of total (69%) and dissolved material (57%) modelled for the outlet node, whereas the Oldman River supplied the majority of total (73%) and dissolved material (59%) during the open season. Seasonal fluctuations for total material contributions from the Bow and Oldman Rivers were more pronounced (i.e. 12-14% greater) than for dissolved material. This seasonal fluctuation is highlighted by a decrease in total material contributions from all but one of the Bow River sites during the open season and an increase from all but two Oldman River sites during the open water season. In particular, the Bow River headwater site (BR1) contributions to total material declined ~20% and three Oldman River tributaries had major increases in source contributions including the Little Bow River (19%), the Oldman River headwaters (14%), and the Saint Mary River (11%). Of these latter tributaries, the 19% increase in the Little Bow River source contributions stands out as this tributary has a relatively gentle topography (i.e. only 5% of the watershed has a slope >10%) compared to the other three sites with montane headwaters.

To facilitate the interpretation of these results, we compiled the mean monthly discharge for 20 of the sites from 1988 to 2018, for which there was a nearby gauging station where the watershed area for the gauging station did not differ from our sites area by more than 11% (Area Ratio (AR) in Table 5). As many of the smaller waterways in this region are essentially frozen or inaccessible during the winter, discharge data was only available for eight of the sites during the ice-covered season. Accordingly, we calculated the annual, ice-covered and open water season mean monthly discharge to contextualize the modelling results where data was available. During our study period, the Bow River supplied 52% of the annual discharge to the South Saskatchewan River relative to the Oldman River's 46%, which is remarkably similar to the contributions modelled with D-MIXSIAR for both total recoverable metals (TRM) and dissolved metals (DM) for the Bow (TRM: 53%, DM 53%) and Oldman Rivers (TRM: 44%, DM: 46%). Additionally, during the ice season, the Bow River supplied 67% of the discharge compared to 69% of the modelled supply of total material and 57% of the supply of dissolved material, whereas in the open season, the Bow River supplied 52% of the discharge compared to only 24% of the modelled total material and 38% of the dissolved material.

Discharge along with the D-MIXSIAR source contributions modelled using total recoverable and dissolved metals for the Bow and Oldman Rivers were relatively similar when examining all annual samples and the ice-covered samples, whereas they clearly deviated during the open water season. In particular, the Oldman River contributed more total material than anticipated based on both watershed area (MCR: 1.58) and more than 1.53 times more than expected based on discharge during the open water season. Much of this increase in total material supply appears to be originating from the Little Bow River which had a 20% increase in its supply of total material during the open season, delivering 1.6 times more total material than its catchment area and ~14 times more than anticipated based on its discharge (Table 7).

One hypothesized driver of the source dynamics of total and dissolved material is the extent of river regulation and irrigation infrastructure in this region. The Bow River watershed is the most regulated catchment in Alberta with 13 dams, four weirs and eight reservoirs (AMEC, 2009). Of note, there are three major impoundments on the main stem of the Bow River between nodes BR1 and BR4. The last major impoundment on the Bow River, Bassano dam, is upstream of node BR4 (the most downstream Bow River sampling node), whereas for the Oldman River, the last main stem impoundment is upstream of the Oldman River headwaters site. There are also several irrigation canals diverting flow along the Bow River from sites BR1 through to BR4 (Figure 1), which are evident as the overall discharge actually decreases in

the open water season between site BR2 (357 million m^3 per month) and site BR4 (297 million m^3 per month).

The decrease in flow and disconnectivity introduced by multiple impoundments on the Bow River logically facilitates the directly related and relative increase in total material supplied to the outlet SSR2 site by the Oldman River. This elevated contribution is likely enhanced by agriculture activities supported by water diversions and irrigation in the Little Bow River watershed and other similar catchments. In particular, there were eight tributary sites with watersheds that had agricultural land uses greater than 50% (Table 8). From these sites, the Little Bow River was found to be a significant contributor of total material in the study area, contributing 20% in the open water season to the downstream outlet site (SSR2) compared to only 1% in the ice-covered season. This high open season contribution from the Little Bow River, which is ~14 times more than expected based on its discharge, is further supported by high total suspended solids (TSS) measurements at this site. During the open season, the Little Bow River had the highest median TSS concentration of all monitored tributary sources (57 mg/L), which is more than double the site with the second highest median open season TSS concentrations (Twelve Mile Coulee - 25 mg/L) (Figure 3). Although the Little Bow River catchment is the largest of the prairie/plain source tributaries, the contribution of total material from the Little Bow River during the open water season is particularly noteworthy when taking into consideration that there is a major reservoir (Travers Reservoir – surface area 22.5 km^2) located ~50 km upstream of the sampling site that is potentially trapping material from ~70% of the Little Bow River watershed. It is likely that enhanced hydrological connectivity derived from agricultural development is facilitating the downstream transport of sediment in the Little Bow River and other similar catchments.

Although the dissolved material source dynamics still varied among the ice-covered and open water seasons, variations were less pronounced. This pattern suggests that the changes in flow conditions and the extensive river regulation throughout the SSRB may have less of an impact on the dissolved material compared to total material. The approach taken to fingerprint sources with dissolved metal concentrations likely only incorporates a fraction of the overall solute load. Ions, nutrients and other dissolved solids likely constitute the majority of material in the dissolved material that was sampled. Although there are likely significant challenges to directly tracing dissolved material with only dissolved metals, this approach has several analogies with tracing the suspended sediments with sediment source fingerprinting techniques. For example, multiple processes occurring in-stream (e.g. sorption, desorption, settling, scouring, etc.) occur within a 'biogeochemical black box' that could affect both the total

recoverable and dissolved metal concentrations potentially adding uncertainty to model results. Nonetheless, the fact that both models behave relatively similarly provides increased confidence in the results, particularly with regards to the potential effect of the major reservoirs trapping potential suspended material relative to the more straightforward downstream migration of the dissolved fraction.

4.3 Perspectives and limitations

This research illustrates a powerful approach to use data generated from water quality monitoring programs to investigate sources of dissolved and total material across large spatial areas (>60,000 km^2). In particular, the D-MIXSIAR model of Blake et al. (2018) is naturally suited to be used with data generated by water quality monitoring programs. Here, the D-MIXSIAR model effectively demonstrated that the majority of the dissolved (76%) and total material (68%) sampled at the outlet of this large catchment is generated in the montane headwater catchments. In addition, it highlighted an interesting seasonal dynamic, where some of the prairie/plains catchments dominated by agriculture, such as the Little Bow River, were modelled to generate a significant and disproportionate amount of total material during the open water season. The results from this research may be used to help optimize Alberta's water quality sampling networks to be more representative of the watersheds that may potentially contribute the majority of total material in this region, and develop targeted focus studies in watersheds that disproportionately contribute material transiting these river systems.

As suspended and dissolved material often act as a proxy for hydro-geomorphological processes operating over multiple scales, this research provides insight into how hydro-geomorphic processes in the Rocky Mountain headwaters drive the flux of dissolved and total material downstream coupled with the disconnectivity introduced by water supply and management infrastructure and the agriculture activities supported by this infrastructure. With multiple dams and reservoirs creating disconnectivity in the downstream transfer of particulate material, future research should analyze metals and fallout radionuclides (i.e. ^{137}Cs, $^{210}Pb_{xs}$, and ^{7}Be) on sediment cores collected in these lentic systems to quantify depositional dynamics and understand how source dynamics have changed over time (e.g. Foucher et al., 2015; Le Gall et al., 2017; Le Gall et al., 2016). The use of next generation tracers such as compound specific stable isotopes (Blake et al., 2012; Mabit et al., 2018; Reiffarth et al., 2019), or even environmental DNA (Evrard et al., 2019; Foucher et al., 2020), may provide more insight into the dominant processes supplying total material in this region.

618 The interdependencies between dissolved and total metal concentrations, along with potential
619 relationships with TSS, may influence model results. There could be situations where variations in TSS may
620 affect estimated source contributions when modelling dissolved and total metal concentrations. These
621 affects will likely be most pronounced for models that unmix individual target samples or those populated
622 with a limited number of source samples. The approach taken in the current research was to capitalize on
623 three years of existent monitoring data to comprehensively model dissolved and total metal distributions
624 for both tributary sources and target material, directly incorporating the variation of TSS throughout the
625 study period. Additionally, we use a distribution approach to address potential non-conservative
626 behaviour in modeled parameters requiring the mean node metal concentrations to plot within one
627 standard deviation of source metal concentrations (Wilkinson et al., 2013). Nonetheless, there are likely
628 situations where non-conservative tracers are still modelled. To help address these non-conservative
629 tracers, our approach was to maximize the number of tracers included in the models (Smith et al., 2018;
630 Wynants et al., 2020), which has been demonstrated to be effective in limiting the affect of non-
631 conservative tracers with Bayesian un-mixing models (Sherriff et al., 2015).

632 Unfortunately, gauging stations were not located near each site and therefore we cannot calculate
633 sediment budgets, sediment loads nor a comprehensive water balance. In the future, water isotopes ($\delta^{16}O$
634 and $\delta^{2}H$) could be utilized to help understand if the water that is driving the generation and transportation
635 of dissolved and total material, is derived from surface runoff due to snowmelt or rainfall, or importantly
636 groundwater sources (Gibson et al., 2005; Stadnyk et al., 2005). The development of multi-tracer
637 approaches that capitalize on a variety of different isotopic fingerprints could provide significant
638 additional information on potential anthropogenic drivers of dissolved and total material source dynamics
639 across the SSRB (Kruk et al., 2020; Laceby et al., 2015b; Tanna et al., 2020).

640 One important caveat when using water quality monitoring data in source fingerprinting research is
641 that quality control data are necessary when analyzing total recoverable and dissolved metals for one-
642 litre grab samples of surface water or potentially even automated stage samples. In particular, not all
643 metals used in mixing models will have equivalent bias or variability. It would be beneficial if future
644 research investigated the potential for bias and variability in sediment and soil samples for a variety of
645 parameters used in sediment source fingerprinting analyses.

646 A second important caveat when utilizing data from water quality monitoring programs in a
647 fingerprinting framework is that the monitoring design will inherently bias model results. For example, in
648 the SSRB, the ice-covered season constitutes five months resulting in essentially ~40% of the annual

649 samples being taken in near base flow conditions. Additionally, ambient water quality monitoring
650 programs are typically not designed to sample different stages of the hydrograph. On the one hand, field
651 staff likely schedule their monthly grab sample campaigns on factors unrelated to streamflow. On the
652 other hand, for basins as large as the SSRB, field staff may at times sample different stages of the
653 hydrograph for different sites in any given month. As such, the base-flow dominance of the ice-covered
654 and the non-hydrograph specific sampling may result in a relatively insignificant portion of the dissolved
655 and total material being modelled to generate the source apportionment results (Horowitz et al., 2008).
656 Although, the model results presented above are likely biased towards the dissolved fraction, differences
657 between the total recoverable and dissolved fraction model results highlight areas that are potentially
658 important sources of particulate matter such as the Little Bow River. Installing multiparameter probes
659 (Clifford et al., 1995; Orwin and Smart, 2005) and time-integrated samplers (Phillips et al., 2000) would be
660 required to thoroughly characterize particulate matter (e.g. sediment) source dynamics across the SSRB.
661 Nonetheless, existent data generated by water quality monitoring programs can be effectively modelled
662 with sediment source fingerprinting approaches to generate a broad-scale understanding the source
663 dynamics of dissolved and total material providing a concrete foundation to develop focus studies
664 addressing issues of concern across a large region such as the SSRB.

665 Future research should investigate the accuracy of the D-MIXSIAR model and the potential
666 conservative behaviour of suspended and dissolved tracing parameters. The generation of synthetic or
667 hypothetical mixtures could help illustrate whether the D-MIXSIAR approach is mathematically robust. In
668 particular, it is important to know how uncertainty in the source contribution in one node may impact
669 other modelled source contributions as they are de-convoluted. Additionally, it would be valuable to
670 understand how the impact of tracer selection affects source contributions modeled by D-MIXSIAR. As
671 the de-convolution of source contributions with D-MIXSIAR is a relatively novel approach in the sediment
672 source fingerprinting literature, we focussed our attention on a new application of the D-MIXSIAR model
673 using data generated by water monitoring programs. Nonetheless, it would be valuable for future
674 research to assess the strengths and limitations of D-MIXSIAR with a robust sensitivity analysis.

675 More research is warranted into the interactions between dissolved and total metals as a multitude of
676 processes occur within the in-stream 'biogeochemical black box' (i.e. exchange processes, sorption,
677 desorption, etc.), which all may affect metal concentrations. In particular, there may be in-stream
678 processes, undocumented sources, and/or other factors driving the non-conservative behaviour of the
679 modelled dissolved and total metals. When modelling source contributions with the sediment

fingerprinting technique, there remains significant uncertainty regarding what actually drives the potential conservative behaviour of parameters populating mixing models (e.g. Motha et al., 2002). Uncertainty in model results driven by the non-conservative behaviour of selected parameters is arguably an under researched theme in the sediment fingerprinting literature. In fact, it is debatable as to whether we should be more or less concerned regarding non-conservative behaviour in the dissolved and total fractions modelled in this current research relative to the potential for the non-conservative behaviour in suspend sediments, sediment cores, lag deposits and rising stage samples. Hopefully, our modelling of the dissolved and total metal parameters in a sediment fingerprinting framework will help instigate more research regarding the potential drivers of non-conservative behaviour in all these various media and present unique opportunities to develop interdisciplinary research collaborations and approaches engaging with surface water and/or groundwater researchers.

5. Conclusion

A significant contribution from this research was the novel use of a water quality monitoring data to investigate the source dynamics of both dissolved and total material in a large-mixed use basin. In particular, a comprehensive quality control program facilitated the inclusion of water quality monitoring data directly into a sediment source fingerprinting framework. As long as researchers have a strong understanding of the quality of their data, particularly for discrete, low volume grab samples of surface water and automated stage samplers, there is significant potential to use water quality data generated from monitoring programs to investigate the source dynamics of dissolved and total material. Additionally, sediment source fingerprinting research could benefit from incorporating quality control best practices from water quality monitoring research and elsewhere to propagate information regarding the uncertainty the data generated (i.e. bias and variability) through mixing models and into the reporting of results. Overall, we believe it is time for researchers fingerprinting sediment sources and those tracing the more soluble fraction to exchange best practices and embark on collaborative research projects investigating source dynamics of the particulate and dissolved loads simultaneously. These collaborations could help further our understanding of how anthropogenic activities may be affecting fundamental critical zone processes and resulting in major changes in the cycling of particulate and dissolved material in riverine systems worldwide.

Acknowledgements

Multiple field, analytical, database and other staff at Alberta Environment and Parks who have supported sampling in the SSRB for the long-term river monitoring network and the tributary monitoring network (TMN) programs over the last 3 years are gratefully acknowledged. Paul Drevnick, David K. Mueller and from multiple anonymous reviewers are thanked for their insightful comments on this manuscript.

References

AAFC, 2018. Annual Space-Based Crop Inventory for Canada 2018, Agriculture and Agri-Food Canada (AAFC), Centre for Agroclimate, Geomatics and Earth Observation, Science and Technology Branch.

AMEC, 2009. South Saskatchewan river basin in Alberta: water supply study. Alberta Agriculture and Rural Development, Lethbridge, Alberta.

Astorga, R.T., de los Santos Villalobos, S., Velasco, H., Domínguez-Quintero, O., Cardoso, R.P., dos Anjos, R.M., Diawara, Y., Dercon, G. and Mabit, L., 2018. Exploring innovative techniques for identifying geochemical elements as fingerprints of sediment sources in an agricultural catchment of Argentina affected by soil erosion. Environmental Science and Pollution Research, 25(21): 20868-20879.

Bahadori, M., Chen, C., Lewis, S., Rashti, M.R., Cook, F., Parnell, A., Esfandbod, M. and Boyd, S., 2019. A novel approach of combining isotopic and geochemical signatures to differentiate the sources of sediments and particulate nutrients from different land uses. Science of The Total Environment, 655: 129-140.

Bainbridge, Z.T., Wolanski, E., Álvarez-Romero, J.G., Lewis, S.E. and Brodie, J.E., 2012. Fine sediment and nutrient dynamics related to particle size and floc formation in a Burdekin River flood plume, Australia. Marine Pollution Bulletin, 65(4–9): 236-248.

Barthod, L.R.M., Liu, K., Lobb, D.A., Owens, P.N., Martínez-Carreras, N., Koiter, A.J., Petticrew, E.L., McCullough, G.K., Liu, C. and Gaspar, L., 2015. Selecting color-based tracers and classifying sediment sources in the assessment of sediment dynamics using sediment source fingerprinting. Journal of environmental quality, 44(5): 1605-1616.

Bender, D.A., Zogorski, J.S., Mueller, D.K., Rose, D.L., Martin, J.D. and Brenner, C.K., 2011. Quality of volatile organic compound data from groundwater and surface water for the National Water-Quality Assessment Program, October 1996–December 2008. 2328-0328, US Geological Survey.

Blake, W.H., Boeckx, P., Stock, B.C., Smith, H.G., Bodé, S., Upadhayay, H.R., Gaspar, L., Goddard, R., Lennard, A.T., Lizaga, I., Lobb DA, PN, O., EL, P., ZZA, K., BD, G., L, M., K, M., A, N., L, M., A, N. and BX, S., 2018. A deconvolutional Bayesian mixing model approach for river basin sediment source apportionment. Scientific Reports, 8:13073(1): 1-12.

Blake, W.H., Ficken, K.J., Taylor, P., Russell, M.A. and Walling, D.E., 2012. Tracing crop-specific sediment sources in agricultural catchments. Geomorphology, 139–140: 322-329.

Boudreault, M., Koiter, A.J., Lobb, D.A., Liu, K., Benoy, G., Owens, P.N. and Li, S., 2019. Comparison of sampling designs for sediment source fingerprinting in an agricultural watershed in Atlantic Canada. Journal of Soils and Sediments.

Brandt, C., Cadisch, G., Nguyen, L.T., Vien, T.D. and Rasche, F., 2016. Compound-specific δ13C isotopes and Bayesian inference for erosion estimates under different land use in Vietnam. Geoderma Regional, 7(3): 311-322.

Bravo-Linares, C., Schuller, P., Castillo, A., Ovando-Fuentealba, L., Muñoz-Arcos, E., Alarcón, O., de los Santos-Villalobos, S., Cardoso, R., Muniz, M. and dos Anjos, R.M., 2018. First use of a compound-specific stable isotope (CSSI) technique to trace sediment transport in upland forest catchments of Chile. Science of The Total Environment, 618: 1114-1124.

Byrne, J., Kienzle, S., Johnson, D., Duke, G., Gannon, V., Selinger, B. and Thomas, J., 2006. Current and future water issues in the Oldman River Basin of Alberta, Canada. Water science and technology, 53(10): 327-334.

Clifford, N., Richards, K., Brown, R. and Lane, S., 1995. Laboratory and field assessment of an infrared turbidity probe and its response to particle size and variation in suspended sediment concentration. Hydrological Sciences Journal, 40(6): 771-791.

763 Collins, A.L., Naden, P.S., Sear, D.A., Jones, J.I., Foster, I.D.L. and Morrow, K., 2011. Sediment targets for
764 informing river catchment management: international experience and prospects. Hydrological
765 processes, 25(13): 2112-2129.
766 Collins, A.L., Zhang, Y., McChesney, D., Walling, D.E., Haley, S.M. and Smith, P., 2012. Sediment source
767 tracing in a lowland agricultural catchment in southern England using a modified procedure
768 combining statistical analysis and numerical modelling. Science of The Total Environment, 414:
769 301-317.
770 Cooper, R.J. and Krueger, T., 2017. An extended Bayesian sediment fingerprinting mixing model for the
771 full Bayes treatment of geochemical uncertainties. Hydrological Processes, 31(10): 1900-1912.
772 Davies, J., Olley, J., Hawker, D. and McBroom, J., 2018. Application of the Bayesian approach to sediment
773 fingerprinting and source attribution. Hydrological processes, 32(26): 3978-3995.
774 Douglas, G., Palmer, M. and Caitcheon, G., 2003. The provenance of sediments in Moreton Bay, Australia:
775 a synthesis of major, trace element and Sr-Nd-Pb isotopic geochemistry, modelling and landscape
776 analysis. Hydrobiologia, 494: 145-152.
777 Downing, D.J. and Pettapiece, W.W., 2006. Natural regions and subregions of Alberta, Natural Regions
778 Committee, Government of Alberta, Edmonton, Alberta.
779 Dutton, C., Anisfeld, S.C. and Ernstberger, H., 2013. A novel sediment fingerprinting method using
780 filtration: Application to the Mara River, East Africa. Journal of soils and sediments, 13(10): 1708-
781 1723.
782 Dyke, A. and Prest, V., 1987. Late Wisconsinan and Holocene history of the Laurentide ice sheet.
783 Géographie physique et Quaternaire, 41(2): 237-263.
784 Elbaz-Poulichet, F., Seidel, J.-L., Casiot, C. and Tusseau-Vuillemin, M.-H., 2006. Short-term variability of
785 dissolved trace element concentrations in the Marne and Seine Rivers near Paris. Science of the
786 Total Environment, 367(1): 278-287.
787 Evrard, O., Laceby, J.P., Ficetola, G.F., Gielly, L., Huon, S., lefèvre, I., Onda, Y. and Poulenard, J., 2019.
788 Environmental DNA provides information on sediment sources: A study in catchments affected
789 by Fukushima radioactive fallout. Science of The Total Environment, 665: 873-881.
790 Fernandez, A., Santos, G.M., Williams, E.K., Pendergraft, M.A., Vetter, L. and Rosenheim, B.E., 2014. Blank
791 corrections for ramped pyrolysis radiocarbon dating of sedimentary and soil organic carbon.
792 Analytical chemistry, 86(24): 12085-12092.
793 Foucher, A., Evrard, O., Ficetola, G.F., Gielly, L., Poulain, J., Giguet-Covex, C., Laceby, J.P., Salvador-Blanes,
794 S., Cerdan, O. and Poulenard, J., 2020. Persistence of environmental DNA in cultivated soils:
795 implication of this memory effect for reconstructing the dynamics of land use and cover changes.
796 Scientific Reports, 10(1): 1-12.
797 Foucher, A., Laceby, J.P., Salvador-Blanes, S., Evrard, O., Le Gall, M., Lefèvre, I., Cerdan, O., Rajkumar, V.
798 and Desmet, M., 2015. Quantifying the dominant sources of sediment in a drained lowland
799 agricultural catchment: The application of a thorium-based particle size correction in sediment
800 fingerprinting. Geomorphology, 250: 271-281.
801 Garzon-Garcia, A., Laceby, J.P., Olley, J.M. and Bunn, S.E., 2017. Differentiating the sources of fine
802 sediment, organic matter and nitrogen in a subtropical Australian catchment. Science of The Total
803 Environment, 575: 1384–1394.
804 Gateuille, D., Evrard, O., Lefevre, I., Moreau-Guigon, E., Alliot, F., Chevreuil, M. and Mouchel, J.-M., 2014.
805 Mass balance and decontamination times of Polycyclic Aromatic Hydrocarbons in rural nested
806 catchments of an early industrialized region (Seine River basin, France). Science of The Total
807 Environment, 470: 608-617.
808 Gellis, A.C. and Walling, D.E., 2011. Sediment Source Fingerprinting (Tracing) and Sediment Budgets as
809 Tools in Targeting River and Watershed Restoration Programs, Stream Restoration in Dynamic

Fluvial Systems: Scientific Approaches, Analyses, and Tools. Geophys. Monogr. Ser. AGU, Washington, DC, pp. 263-291.
Gibson, J.J., Edwards, T.W.D., Birks, S.J., St Amour, N.A., Buhay, W.M., McEachern, P., Wolfe, B.B. and Peters, D.L., 2005. Progress in isotope tracer hydrology in Canada. Hydrological Processes: An International Journal, 19(1): 303-327.
Glendell, M., Jones, R., Dungait, J.A.J., Meusburger, K., Schwendel, A.C., Barclay, R., Barker, S., Haley, S., Quine, T.A. and Meersmans, J., 2018. Tracing of particulate organic C sources across the terrestrial-aquatic continuum, a case study at the catchment scale (Carminowe Creek, southwest England). Science of The Total Environment, 616-617: 1077-1088.
Godwin, R. and Martin, F., 1975. Calculation of gross and effective drainage areas for the Prairie Provinces, Canadian Hydrology Symposium-1975 Proceedings, 11-14 August 1975, Winnipeg, Manitoba, pp. 219-223.
Grasby, S., Hutcheon, I. and Krouse, H., 1997. Application of the stable isotope composition of S04 to tracing anomalous TDS in Nose Creek, southern Alberta, Canada. Applied geochemistry, 12(5): 567-575.
Grasby, S.E. and Hutcheon, I., 2000. Chemical dynamics and weathering rates of a carbonate basin Bow River, southern Alberta. Applied Geochemistry, 15(1): 67-77.
Guzmán, G., Barrón, V. and Gómez, J.A., 2010. Evaluation of magnetic iron oxides as sediment tracers in water erosion experiments. CATENA, In Press, Corrected Proof.
Halliday, R., 2009. From the mountains to the sea: The state of the Saskatchewan River Basin. Partners for the Saskatchewan River Basin, Saskatoon.
Hamilton, W., Price, M. and Langenberg, C., 1999. Geological map of Alberta: Alberta Geological Survey. Alberta Energy Utilities Board, Map, 236(1): 1,000,000.
Hatfield, R.G. and Maher, B.A., 2008. Suspended sediment characterization and tracing using a magnetic fingerprinting technique: Bassenthwaite Lake, Cumbria, UK. The Holocene, 18(1): 105-115.
Hooke, R.L., Martín-Duque, J.F. and Pedraza, J., 2012. Land transformation by humans: a review. GSA today, 22(12): 4-10.
Horowitz, A.J., Elrick, K.A. and Smith, J.J., 2008. Monitoring urban impacts on suspended sediment, trace element, and nutrient fluxes within the City of Atlanta, Georgia, USA: program design, methodological considerations, and initial results. Hydrological Processes, 22(10): 1473-1496.
Jalowska, A.M., McKee, B.A., Laceby, J.P. and Rodriguez, A.B., 2017. Tracing the sources, fate, and recycling of fine sediments across a river-delta interface. Catena, 154: 95-106.
Jantzi, S.C., Dutton, C.L., Saha, A., Masikini, R. and Almirall, J.R., 2019. Novel “filter pellet” sample preparation strategy for quantitative LA-ICP-MS analysis of filter-bound sediments: a “green chemistry” alternative to sediment fingerprinting in Tanzania’s Ruvu River basin. Journal of soils and sediments, 19(1): 478-490.
Kerr, J.G., 2017. Multiple land use activities drive riverine salinization in a large, semi-arid river basin in western Canada. Limnology and Oceanography, 62(4): 1331-1345.
Klages, M.G. and Hsieh, Y.P., 1975. Suspended solids carried by the Gallatin River of southwestern Montana: II. Using minerology for inferring sources. Journal of Environmental Quality, 4(1): 68-73.
Koiter, A., Lobb, D., Owens, P., Petticrew, E., Tiessen, K.D. and Li, S., 2013. Investigating the role of connectivity and scale in assessing the sources of sediment in an agricultural watershed in the Canadian prairies using sediment source fingerprinting. Journal of Soils and Sediments, 13(10): 1676-1691.
Koning, C.W., Saffran, K.A., Little, J.L. and Fent, L., 2006. Water quality monitoring: the basis for watershed management in the Oldman River Basin, Canada. Water science and technology, 53(10): 153-161.

Kraushaar, S., Schumann, T., Ollesch, G., Schubert, M., Vogel, H.-J. and Siebert, C., 2015. Sediment fingerprinting in northern Jordan: element-specific correction factors in a carbonatic setting. Journal of Soils and Sediments, 15(10): 2155-2173.

Kruk, M., Mayer, B., Nightingale, M. and Laceby, J.P., 2020. Tracing nitrate sources with a combined isotope approach (δ15NNO3, δ18ONO3 and δ11B) in a large mixed-use watershed in Southern Alberta, Canada. Science of The Total Environment, 703: 1-15.

Laceby, J.P., Chung, C., Kruk, M.K. and Kerr, J.G., in press. Investigation of quality control data from Alberta's lotic water monitoring programs, 2016-2018, Alberta Environment and Parks, Edmonton, Canada.

Laceby, J.P., Evrard, O., Smith, H., Blake, W., Olley, J., Minella, J.P.G. and Owens, P.N., 2017. The challenges and opportunities of addressing particle size effects in sediment source fingerprinting: a review. Earth-Science Reviews, 169: 85–103.

Laceby, J.P., McMahon, J., Evrard, O. and Olley, J., 2015a. A comparison of geological and statistical approaches to element selection for sediment fingerprinting. Journal of Soils and Sediments, 15(10): 2117-2131.

Laceby, J.P., Olley, J., Pietsch, T.J., Sheldon, F. and Bunn, S.E., 2015b. Identifying subsoil sediment sources with carbon and nitrogen stable isotope ratios. Hydrological Processes, 29(8): 1956-1971.

Le Gall, M., Evrard, O., Foucher, A., Laceby, J.P., Salvador-Blanes, S., Manière, L., Lefèvre, I., Cerdan, O. and Ayrault, S., 2017. Investigating the temporal dynamics of suspended sediment during flood events with ^{7}Be and $^{210}Pb_{xs}$ measurements in a drained lowland catchment. Scientific Reports, 7: 1-10.

Le Gall, M., Evrard, O., Foucher, A., Laceby, J.P., Salvador-Blanes, S., Thil, F., Dapoigny, A., Lefèvre, I., Cerdan, O. and Ayrault, S., 2016. Quantifying sediment sources in a lowland agricultural catchment pond using ^{137}Cs activities and radiogenic $^{87}Sr/^{86}Sr$ ratios. Science of The Total Environment, 566–567: 968-980.

Lewin, J. and Wolfenden, P.J., 1978. The assessment of sediment sources: A field experiment. Earth Surface Processes 3: 171-178.

Liu, K., Lobb, D.A., Miller, J.J., Owens, P.N. and Caron, M.E.G., 2017. Determining sources of fine-grained sediment for a reach of the Lower Little Bow River, Alberta, using a colour-based sediment fingerprinting approach. Canadian journal of soil science, 98(1): 55-69.

Lizaga Villuendas, I., Latorre Garcés, B., Gaspar Ferrer, L. and Navas Izquierdo, A., 2018. FingerPro mixing model: An R package for sediment tracing.

Mabit, L., Gibbs, M., Mbaye, M., Meusburger, K., Toloza, A., Resch, C., Klik, A., Swales, A. and Alewell, C., 2018. Novel application of Compound Specific Stable Isotope (CSSI) techniques to investigate on-site sediment origins across arable fields. Geoderma, 316: 19-26.

McCarney-Castle, K., Childress, T.M. and Heaton, C.R., 2017. Sediment source identification and load prediction in a mixed-use Piedmont watershed, South Carolina. Journal of Environmental Management, 185: 60-69.

Meybeck, M., 2003. Global analysis of river systems: from Earth system controls to Anthropocene syndromes. Philosophical Transactions of the Royal Society of London. Series B: Biological Sciences, 358(1440): 1935-1955.

Meybeck, M. and Helmer, R., 1989. The quality of rivers: from pristine stage to global pollution. Palaeogeography, Palaeoclimatology, Palaeoecology, 75(4): 283-309.

Motha, J.A., Wallbrink, P.J., Hairsine, P.B. and Grayson, R.B., 2002. Tracer properties of eroded sediment and source material. Hydrological Processes, 16: 1983-2000.

Mueller, D.K., Martin, J. and Lopes, T.J., 1997. Quality-control design for surface-water sampling in the National Water-Quality Assessment Program. US Geological Survey Reston, VA.

Mueller, D.K., Schertz, T.L., Martin, J.D. and Sandstrom, M.W., 2015. Design, analysis, and interpretation of field quality-control data for water-sampling projects. 2328-7055, US Geological Survey (From: https://pubs.er.usgs.gov/publication/tm4C4).

Oldfield, F., Rummery, T.A., Thompson, R. and Walling, D.E., 1979. Identification of suspended sediment sources by means of magnetic measurements: Some preliminary results. Water Resources Research, 15(2): 211-218.

Orwin, J.F. and Smart, C.C., 2005. An inexpensive turbidimeter for monitoring suspended sediment. Geomorphology, 68(1-2): 3-15.

Parnell, A., Inger, R., Bearhop, S. and Jackson, A.L., 2008. Stable isotope analysis in R (SIAR).

Phillips, J.M., Russell, M.A. and Walling, D.E., 2000. Time-integrated sampling of fluvial suspended sediment: a simple methodology for small catchments. Hydrological Processes, 14(14): 2589-2602.

Pomeroy, J., de Boer, D. and Martz, L., 2005. Hydrology and water resources of Saskatchewan. Centre for Hydrology, University of Saskatchewan Saskatoon.

Pulley, S. and Collins, A., 2018. Tracing catchment fine sediment sources using the new SIFT (SedIment Fingerprinting Tool) open source software. Science of the Total Environment, 635: 838-858.

R Development Core Team, 2011. R: A language and environment for statistical computing, Vienna, Austria.

Reiffarth, D.G., Petticrew, E.L., Owens, P.N. and Lobb, D.A., 2019. Spatial differentiation of cultivated soils using compound-specific stable isotopes (CSSIs) in an agricultural watershed in Manitoba, Canada. Journal of Soils and Sediments.

Richter, D. and Mobley, M.L., 2009. Monitoring Earth's critical zone. Science, 326(5956): 1067-1068.

Riskin, M.L., Reutter, D.C., Martin, J.D. and Mueller, D.K., 2018. Quality-control design for surface-water sampling in the National Water-Quality Network. 2331-1258, US Geological Survey.

Sanisaca, L.E.G., Gellis, A.C. and Lorenz, D.L., 2017. Determining the sources of fine-grained sediment using the Sediment Source Assessment Tool (Sed_SAT). 2331-1258, US Geological Survey.

Schindler, D.W. and Donahue, W.F., 2006. An impending water crisis in Canada's western prairie provinces. Proceedings of the National Academy of Sciences, 103(19): 7210-7216.

Semmens, B.X., Stock, B., Ward, E., Moore, J.W., Parnell, A., Jackson, A.L., Phillips, D.L., Bearhop, S. and Inger, R., 2013. MixSIAR: A Bayesian stable isotope mixing model for characterizing intrapopulation niche variation. Ecological Society of America, Minneapolis, MN, 04-09.

Sherriff, S.C., Franks, S.W., Rowan, J.S., Fenton, O. and Ó'hUallacháin, D., 2015. Uncertainty-based assessment of tracer selection, tracer non-conservativeness and multiple solutions in sediment fingerprinting using synthetic and field data. Journal of Soils and Sediments, 10: 2101-2116.

Small, I.F., Rowan, J.S. and Franks, S.W., 2002. Quantitative sediment fingerprinting using a Bayesian uncertainty estimation framework. International Association of Hydrological Sciences, Publication, 276: 443-450.

Smith, H.G., Karam, D.S. and Lennard, A.T., 2018. Evaluating tracer selection for catchment sediment fingerprinting. Journal of soils and sediments, 18(9): 3005-3019.

Stadnyk, T., Amour, N.S., Kouwen, N., Edwards, T.W.D., Pietroniro, A. and Gibson, J.J., 2005. A groundwater separation study in boreal wetland terrain: The WATFLOOD hydrological model compared with stable isotope tracers. Isotopes in Environ Health Studies, 41(1): 49-68.

Statistics Canada, 2017. Agricultural Water Survey, 2016, Irrigation volume by province and drainage region, Table: 38-10-0239-01, Ottawa, from: https://www150.statcan.gc.ca/n1/daily-quotidien/170908/dq170908c-eng.htm, retrieved January 23, 2020.

Stock, B.C., Jackson, A.L., Ward, E.J., Parnell, A.C., Phillips, D.L. and Semmens, B.X., 2018. Analyzing mixing systems using a new generation of Bayesian tracer mixing models. PeerJ, 6: e5096.

Stock, B.C. and Semmens, B.X.J.A.o.a.h.c.i.-c.o.u.b.s.M., 2013. MixSIAR GUI user manual, version 1.0.

Tanna, R.N., Moncur, M.C., Birks, S.J., Gibson, J.J., Ptacek, C.J., Mayer, B., Wieser, M.E., Wrona, F.J. and Munkittrick, K.R., 2020. Utility of a multi-tracer approach as a component of adaptive monitoring for municipal wastewater impacts. Water Quality Research Journal, 55(3): 327-341.

Tiecher, T., Ramon, R., Laceby, J.P., Evrard, O. and Minella, J.P.G., 2019. Potential of phosphorus fractions to trace sediment sources in a rural catchment of Southern Brazil: comparison with the conventional approach based on elemental geochemistry. Geoderma, 337: 1067-1076.

Upadhayay, H.R., Bodé, S., Griepentrog, M., Bajracharya, R.M., Blake, W., Cornelis, W. and Boeckx, P., 2018a. Isotope mixing models require individual isotopic tracer content for correct quantification of sediment source contributions. Hydrological processes, 32(7): 981-989.

Upadhayay, H.R., Smith, H.G., Griepentrog, M., Bodé, S., Bajracharya, R.M., Blake, W., Cornelis, W. and Boeckx, P., 2018b. Community managed forests dominate the catchment sediment cascade in the mid-hills of Nepal: A compound-specific stable isotope analysis. Science of the Total Environment, 637: 306-317.

Walling, D.E., Woodward, J.C. and Nicholas, A.P., 1993. A multi-parameter approach to fingerprinting suspended-sediment sources. In: N.E. Peters, E. Hoehn, C. Leibundgut, N. Tase and D.E. Walling (Editors), Tracers in Hydrology, IAHS Publication No. 215, IAHS Press, Wallingford, pp. 329-338.

Wilkinson, S., Hancock, G., Bartley, R., Hawdon, A. and Keen, R., 2013. Using sediment tracing to assess processes and spatial patterns of erosion in grazed rangelands, Burdekin River basin, Australia. Agriculture, Ecosystems & Environment, 180: 90-102.

Wynants, M., Millward, G., Patrick, A., Taylor, A., Munishi, L., Mtei, K., Brendonck, L., Gilvear, D., Boeckx, P., Ndakidemi, P. and Blake, W.H., 2020. Determining tributary sources of increased sedimentation in East-African Rift Lakes. Science of The Total Environment, 717: 137266.

Figures and Tables

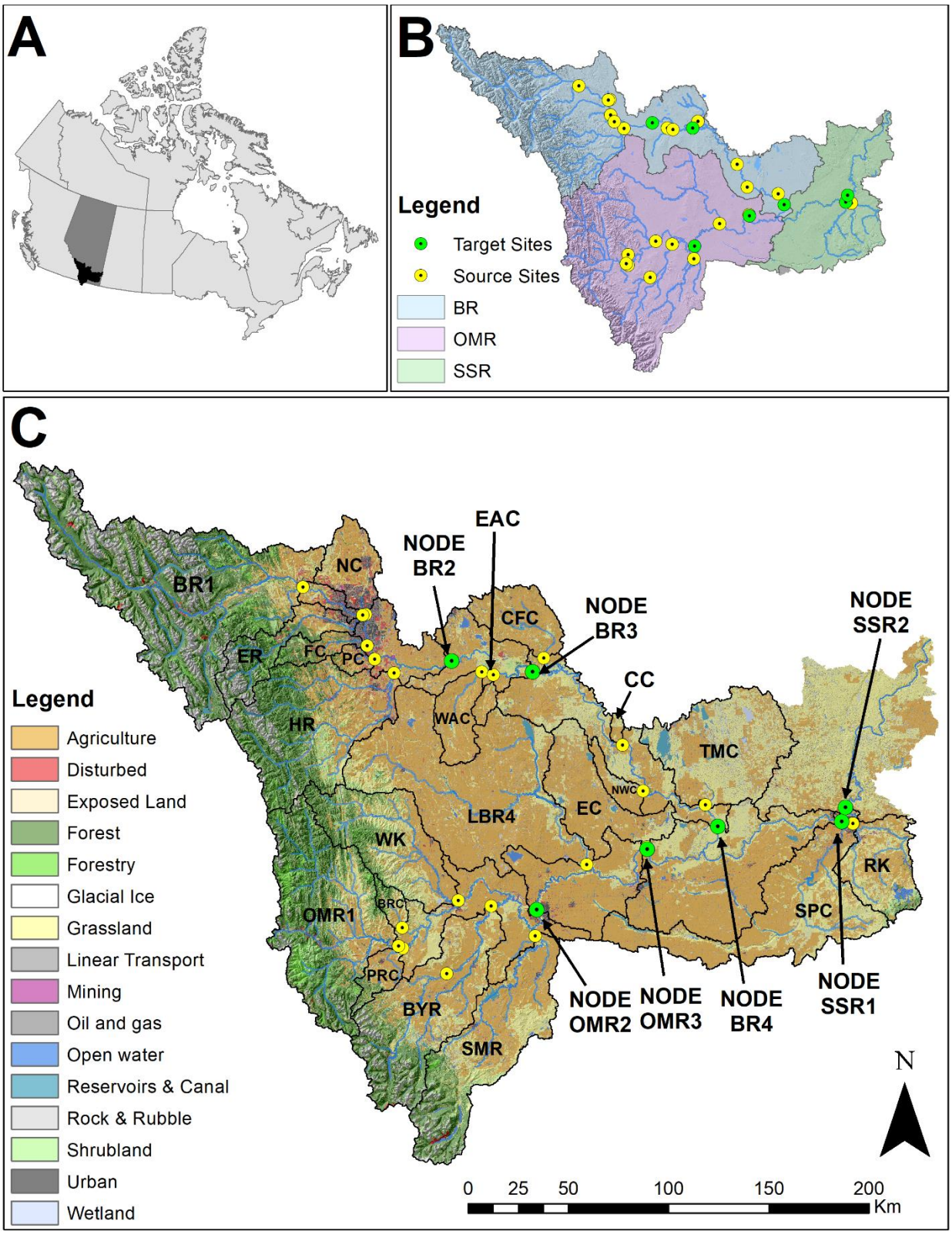

Figure 1: Location of the SSRB in Canada (inset A), the confluence of the Bow River (BR) and the Oldman Rivers (OMR) (inset B), along with the tributary and node sites / watersheds overlain on land use / land cover for the study region (C).

981

Table 1: Summary of sampling information for each site including site name, site identification (ID), basin, latitude, longitude, node information and the number of samples taken at each site including the ice-covered (November – March) and open-water (April – October) seasons.

Site Name	Basin	ID	Area (km2)	Latitude	Longitude	Mix	Node	*n samples*		
								Total	Ice	Open
Bow River @ Cochrane	BR	BR1	7543	51.1831	114.4871		1	33	12	21
Bow River D/S Carseland Dam	BR	BR2	15585	50.8306	113.4167	1	1	33	12	21
Elbow River	BR	ER	1240	51.0448	114.0419		1	33	12	21
Fish Creek	BR	FC	443	50.9052	114.0110		1	26	6	20
Highwood River	BR	HR	3948	50.7823	113.8259		1	32	12	20
Nose Creek	BR	NC	948	51.0464	114.0189		1	31	11	20
Pine Creek	BR	PC	210	50.8450	113.9619		1	27	7	20
Bow River @ Cluny	BR	BR3	17826	50.7731	112.8455	2	2	33	12	21
East Arrowwood Creek	BR	EAC	165	50.7647	113.1239		2	21	1	20
West Arrowwood Creek	BR	WAC	813	50.7792	113.2036		2	15	1	14
Bow River @ Ronalane Bridge	BR	BR4	24766	50.0478	111.4248	3	3	33	12	21
Coal Creek	BR	CC	76	50.4306	112.2278		3	21	1	20
Crowfoot Creek	BR	CFC	1068	50.8333	112.7611		3	21	1	20
New West Coulee	BR	NWC	352	50.2167	112.0208		3	21	1	20
Twelve Mile Creek	BR	TMC	2958	50.1500	111.6667		3	20	1	19
Beaver Creek	OMR	BRC	256	49.6393	113.7952		4	23	2	21
Belly River	OMR	BYR	3614	49.7275	113.1781		4	32	11	21
Oldman River @ Brocket	OMR	OMR1	4369	49.5586	113.8222		4	33	12	21
Oldman River U/S Lethbridge	OMR	OMR2	16800	49.7067	112.8629	4	4	32	11	21
Pincher Creek	OMR	PRC	425	49.5463	113.7945		4	28	8	20
St. Mary River	OMR	SMR	3440	49.5889	112.8806		4	31	10	21
Willow Creek	OMR	WK	2506	49.7572	113.4069		4	23	2	21
Little Bow River	OMR	LBR4	5890	49.9017	112.5067		5	32	11	21
Oldman River @ Taber	OMR	OMR3	24691	49.9611	112.0847	5	5	32	11	21
Expanse Coulee	OMR	EC	1859	49.9717	112.0833		6	23	2	21
Ross Creek	SSR	RK	1452	50.0311	110.6431		6	30	10	20
Seven Persons Creek	SSR	SPC	3473	50.0311	110.6439		7	30	10	20
SSR U/S Medicine Hat	SSR	SSR1	55345	50.0433	110.7222	6	7	33	12	21
SSR D/S Medicine Hat	SSR	SSR2	60330	50.1048	110.6911	7	7	30	10	20

Table 2: Results from the analysis of blank and duplicate samples for total recoverable metals in the SSRB including the field blank detection (detect) frequency, the potential environmental contamination, the 90-percent UCL for the percentage of inconsistent detects, and the mean confidence interval (M-CI) for the duplicate samples. Any variable with greater than 20% for the potential environmental contamination, the UCL of inconsistent detections or the M-CI was not selected for modelling which is denoted by the asterisks (*) beside the percentages.

Metal	Detection Frequency (%)	Pot. Env. Cont. (%)	90-percent UCL for % Inconsistent Detects	M-CI (%)	Modelled
Aluminum (Al)	88	9	2	21*	
Antimony (Sb)	20	1	2	6	Yes
Arsenic (As)	20	0	2	10	Yes
Barium (Ba)	40	0	2	3	Yes
Beryllium (Be)	2	4	20*	32*	
Bismuth (Bi)	7	12	28*	59*	
Boron (B)	40	0	2	4	Yes
Cadmium (Cd)	4	8	17	54*	
Calcium (Ca)	38	0	2	3	Yes
Chlorine (Cl)	57	21*	2	7	
Chromium (Cr)	21	2	19	40*	
Cobalt (Co)	20	4	2	21*	
Copper (Cu)	52	31*	2	18	
Iron (Fe)	52	4	2	15	Yes
Lead (Pb)	51	20*	2	23*	
Lithium (Li)	18	0	2	4	Yes
Manganese (Mn)	41	0	2	11	Yes
Molybdenum(Mo)	54	0	2	5	Yes
Nickel (Ni)	42	5	3	28*	
Selenium (Se)	5	2	3	23*	
Silver (Ag)	10	4	17	81*	
Strontium (Sr)	37	0	2	3	Yes
Thallium (Tl)	11	8	3	45*	
Thorium (Th)	19	7	4	41*	
Tin (Sn)	36	2	12	52*	
Titanium (Ti)	46	14	2	21*	
Uranium (U)	9	0	2	3	Yes
Vanadium (V)	28	6	2	15	Yes
Zinc (Zn)	63	37*	2	33*	

* Indicates percentage greater than 20 resulting in these metals not being modelled

Table 3: Metals that passed the conservative bracket/range test for each of the seven nodes in the SSRB and for each of the three different modelling scenarios (i.e. all samples, the open season and the ice season). Metal abbreviations are provided in Table 2 or the periodic table.

Type	Node 1 - BR2			Node 2 - BR3			Node 3 - BR4			Node 4 - OMR2			Node 5 - OMR3			Node 6 - SSR1			Node 7 - SSR2		
	All	**Open**	**Ice**	**All**	**Open**	**Ice**	**All**	**Open**	**Ice**	**All**	**Open**	**Ice**	**All**	**Open**	**Ice**	**All**	**Open**	**Ice**	**All**	**Open**	**Ice**
Total R. Metals	As	As	As	As	As	As	B	As	B	As	As	As	As	As	As	As	B	As	As	As	B
	B	B	B	B	B	B	Ca	B	Ba	B	B	B	B	Ba	B	B	Ca	B	B	B	Ba
	Ba	Ba	Ba	Li	Ba	Ca	Li	Ba	Ca	Ba	Ba	Ba	Ba	Ca	Ba	Ca	Li	Ba	Ba	Ba	Ca
	Ca	Ca	Ca	Sb	Fe	Fe	Mo	Li	Li	Ca	Ca	Ca	Ca	Mo	Ca	Li	Mo	Ca	Ca	Ca	Mo
	Fe	Fe	Fe	U	Li	Li	Sb	Mn	Mn	Fe	Fe	Fe	Li	Sb	Fe	Mn	Sb	Fe	Fe	Fe	Sb
	Li	Li	Li		Mn	Mo	Sr	Mo	Mo	Li	Li	Li	Mo	Sr	Li	Mo	Sr	Li	Li	Li	Sr
	Mn	Mn	Mn		Sb	Sb	U	Sb	Sb	Mn	Mn	Mn	Sb		Mn	Sb		Mn	Mn	Mn	U
	Mo	Mo	Mo		Sr	Sr		Sr	Sr	Mo	Mo	Mo	Sr		Mo	Sr		Mo	Mo	Mo	V
	Sb	Sb	Sb		U	U		U	U	Sb	Sb	Sb	U		Sb	U		Sr	Sb	Sb	
	Sr	Sr	Sr		V	V		V		Sr	Sr	Sr			Sr			U	Sr	Sr	
	U	U	U							U	U	U			U			V	U	U	
	V	V	V							V	V	V			V				V	V	
Dissolved Metals	As	As	As	As	As	As	B	As	As	As	As	As	As	As	As	As	As	As	As	As	As
	B	B	B	B	Ba	B	Ba	B	B	B	B	B	B	B	B	B	B	B	B	B	B
	Ba	Ba	Ba	Cl	Li	Cl	Ca	Ba	Ba	Ba	Ba	Ba	Ba	Ba	Ba	Ba	Ba	Ba	Ba	Ba	Ba
	Ca	Ca	Ca	Li	V	Li	Li	Ca	Ca	Ca	Ca	Ca	Ca	Cl	Ca	Ca	Ca	Ca	Ca	Ca	Ca
	Cl	Cl	Cl	Sb		Sb	Mo	Li	Li	Cl	Cl	Cl	Li	Li	Li	Cl	Cl	Cl	Li	Li	Li
	Li	Li	Li	U		U	Sb	Mo	Mo	Li	Li	Li	Mo	Mo	Mo	Li	Li	Li	Mo	Mo	Mo
	Mo	Mo	Mo	V		V	Sr	Sb	Sb	Mo	Mo	Mo	Sb	Sb	Sb	Mo	Mo	Mo	Sb	Sb	Sb
	Sb	Sb	Sb				U	Sr	Sr	Sb	Sb	Sb	Sr	Sr	Sr	Sb	Sb	Sb	Sr	Sr	Sr
	Sr	Sr	Sr					U		Sr	Sr	Sr	U	U	U	Sr	Sr	Sr	U	V	U
	U	U	U							U	U	U	V	V	V	U	U	U	V		V
	V	V	V							V	V	V				V	V	V			

Table 4: Results from the analysis for blank and duplicate samples for dissolved metals the SSRB including the field blank detection (detect) frequency, the potential environmental contamination, the 90-percent UCL for the percentage of inconsistent detects, and the mean confidence interval (M-CI) for the duplicate samples. Any variable with greater than 20% for the potential environmental contamination, the UCL of inconsistent detections or the M-CI was not selected for modelling which is denoted by the asterisks (*) beside the percentages.

Metal	Detection Frequency (%)	Pot. Env. Cont. (%)	90-percent UCL for % Inconsistent Detects	M-CI (%)	Modelled
Aluminum (Al)	58	28*	5	38*	
Antimony (Sb)	0	0	3	8	Yes
Arsenic (As)	17	0	2	10	Yes
Barium (Ba)	2	0	2	2	Yes
Beryllium (Be)	2	3	94*	9	
Bismuth (Bi)	0	0	92*	38*	
Boron (B)	35	0	2	4	Yes
Cadmium (Cd)	2	3	11	47*	
Calcium (Ca)	0	0	2	4	Yes
Chlorine (Cl)	30	14	3	9	Yes
Chromium (Cr)	0	0	55*	111*	
Cobalt (Co)	6	0	4	32*	
Copper (Cu)	24	20*	2	14	
Iron (Fe)	26	0	9	42*	
Lead (Pb)	13	2	20*	58*	
Lithium (Li)	17	0	2	4	Yes
Manganese (Mn)	41	2	2	35*	
Molybdenum (Mo)	27	0	2	4	Yes
Nickel (Ni)	32	2	3	30*	
Selenium (Se)	3	0	5	24*	
Silver (Ag)	7	0	40*	91*	
Strontium (Sr)	3	0	2	3	Yes
Thallium (Tl)	16	0	12	45*	
Thorium (Th)	19	6	19	56*	
Tin (Sn)	27	0	18	51*	
Titanium (Ti)	38	21*	3	18*	
Uranium (U)	7	0	2	3	Yes
Vanadium (V)	4	1	2	18	Yes
Zinc (Zn)	41	9	9	42*	

* Indicates percentage greater than 20 resulting in these metals not being modelled

Table 5: The dissolved to total recoverable ratio (DTR) for all analyzed metals across a range of total suspended solids concentrations (Low TSS: <50 mg/L, Medium TSS: 50-100 mg/L, High TSS (100-1000 mg/L) and very high TSS (>1000 mg/L). For example, Ag for all samples has a DTR of 51% indicating that half of the material in the total recoverable ratio is in dissolved form.

Metal	n	All DTR (%)	n Low TSS	Low TSS DTR (%)	n Medium TSS	Medium TSS DTR (%)	n High TSS	High TSS DTR (%)	n Very High TSS	Very High TSS DTR (%)
Ag	229	51	188	59	16	19	23	11	2	3
Al	816	6	725	7	42	1	45	0	4	0
As*	848	80	756	84	43	64	45	38	4	12
B*	848	95	756	96	43	96	45	90	4	70
Ba*	848	89	756	92	43	74	45	57	4	11
Be	49	54	39	64	4	18	5	16	1	1
Bi	100	81	88	86	7	45	4	52	1	3
Ca*	848	98	756	99	43	97	45	85	4	33
Cd	604	50	515	55	42	21	43	12	4	2
Cl	844	97	754	97	43	98	43	97	4	97
Co	780	48	689	53	42	18	45	8	4	1
Cr	232	61	206	67	14	17	11	12	1	1
Cu	847	72	755	77	43	40	45	27	4	6
Fe*	725	8	639	9	40	2	42	1	4	0
Li*	848	94	756	96	43	90	45	70	4	32
Mn*	844	16	752	18	43	6	45	2	4	0
Mo*	848	98	756	98	43	98	45	100	4	99
Ni	813	67	723	71	42	51	44	30	4	7
Pb	501	20	437	22	29	4	31	2	4	0
Sb*	720	96	636	97	41	97	39	87	4	93
Se	835	90	747	91	43	85	41	81	4	45
Sn	321	81	283	83	17	69	20	64	1	100
Sr*	848	96	756	97	43	96	45	89	4	57
Th	641	39	559	44	37	14	41	5	4	1
Ti	821	25	731	27	41	9	45	5	4	5
Tl	779	64	694	70	37	24	44	18	4	6
U*	848	95	756	97	43	93	45	79	4	50
V*	847	49	755	53	43	23	45	10	4	3
Zn	794	48	710	52	40	13	40	9	4	1

* indicates metals may have been selected in the modelling of total recoverable metals

Table 6: D-con model results including the mean (M) and standard deviation (SD) of the 22 tributary site contributions to total and dissolved material sampled at outlet node sample SSR2 including the mean contribution ratio (MCR).

Site	Total - All samples			Dissolved - All samples			Total – Ice-covered			Dissolved – Ice-covered			Total - Open Water			Dissolved - Open Water		
	M	SD	MCR	M	SD	MCR	M	SD	MCR	M	SD	MCR	M	SD	MCR	M	SD	MCR
BR1	27%	8%	1.68	31%	6%	1.92	31%	8%	1.94	29%	7%	1.78	11%	7%	0.69	22%	8%	1.38
ER	1%	1%	0.38	1%	1%	0.53	4%	4%	1.52	4%	4%	1.48	0%	1%	0.15	1%	1%	0.46
FC	1%	1%	0.64	1%	1%	0.64	1%	1%	1.49	1%	1%	1.28	0%	0%	0.32	1%	1%	0.53
HR	6%	3%	0.72	5%	3%	0.62	7%	5%	0.86	6%	5%	0.73	2%	2%	0.19	3%	2%	0.33
NC	2%	1%	0.99	1%	1%	0.65	3%	2%	1.34	2%	1%	0.84	1%	1%	0.40	1%	1%	0.40
PC	1%	1%	1.12	1%	1%	2.46	2%	2%	4.93	2%	2%	4.26	0%	0%	0.67	1%	1%	1.57
EAC	0%	0%	0.86	0%	0%	0.86	1%	1%	3.42	1%	1%	3.14	0%	0%	1.14	1%	1%	2.00
WAC	0%	0%	0.17	0%	0%	0.12	1%	1%	0.75	1%	1%	0.46	0%	0%	0.12	0%	0%	0.23
CC	2%	1%	9.85	2%	2%	12.3	4%	3%	24.0	3%	3%	17.9	1%	1%	6.16	2%	2%	10.5
CFC	3%	2%	1.50	2%	1%	0.75	2%	2%	1.01	2%	2%	0.84	2%	2%	1.01	1%	1%	0.62
NWC	7%	4%	9.22	5%	3%	6.41	7%	6%	9.75	5%	4%	6.14	3%	3%	3.74	3%	2%	3.61
TMC	4%	3%	0.62	3%	2%	0.51	4%	4%	0.70	3%	2%	0.45	3%	3%	0.41	3%	2%	0.43
BRC	1%	1%	0.92	1%	1%	1.10	0%	1%	0.74	0%	0%	0.74	1%	1%	2.02	1%	1%	1.84
BYR1	9%	5%	1.22	15%	5%	1.94	9%	6%	1.18	16%	7%	2.02	12%	5%	1.50	16%	8%	2.04
OMR1	12%	5%	1.28	14%	5%	1.55	5%	4%	0.48	10%	5%	1.02	18%	6%	1.97	21%	7%	2.22
PC1	2%	2%	2.65	3%	2%	2.88	2%	2%	1.66	2%	2%	2.54	4%	3%	3.98	2%	2%	2.32
SMR	8%	4%	1.11	5%	4%	0.70	2%	2%	0.30	2%	2%	0.31	14%	6%	1.85	9%	6%	1.27
WK	1%	1%	0.23	1%	1%	0.13	1%	1%	0.11	1%	1%	0.11	2%	2%	0.41	1%	1%	0.23
LBR	9%	4%	0.71	7%	3%	0.53	1%	1%	0.09	2%	2%	0.16	20%	7%	1.61	9%	4%	0.68
EC	2%	1%	0.51	1%	1%	0.15	3%	2%	0.73	1%	1%	0.30	3%	2%	0.73	1%	1%	0.23
RK	1%	1%	0.29	1%	1%	0.26	4%	3%	1.26	4%	3%	1.26	1%	1%	0.42	1%	1%	0.45
SPC	1%	1%	0.18	1%	1%	0.12	5%	4%	0.61	5%	4%	0.65	2%	2%	0.26	2%	1%	0.20

Table 7: Mean monthly discharge for the open water and ice-covered seasons from the closest available gauging station operated by the Water Survey of Canada with an area ratio (AR) maximum between the gauging station and the sampling site of 11%.

Site Name	ID	Gauge Stations		n samples (1998-2018)		Discharge (in million m^3 per month)	
		ID	AR (%)	Open	Ice	Open	Ice
Bow River @ Cochrane	BR1	05BH005	2	374	71	312	--
Bow River D/S Carseland Dam	BR2	05BM002	0	611	6	357	--
Elbow River	ER	05BJ001	0	581	575	30	7
Fish Creek	FC	--	--	--	--	--	--
Highwood River	HR	05BL024	0	581	575	86	11
Nose Creek	NC	--	--	--	--	--	--
Pine Creek	PC	--	--	--	--	--	--
Bow River @ Cluny	BR3	--	--	--	--	--	--
East Arrowwood Creek	EAC	--	--	--	--	--	--
West Arrowwood Creek	WAC	05BM014	4	581	229	1	--
Bow River @ Ronalane Bridge	BR4	05BN012	2	642	635	298	164
Coal Creek	CC	--	--	--	--	--	--
Crowfoot Creek	CFC	05BM008	3	642	133	5	--
New West Coulee	NWC	05BN006	10	642	5	3	--
Twelve Mile Creek	TMC	05BN002	6	556	2	5	--
Beaver Creek	BRC	05AB013	0	611	126	1	--
Belly River	BYR	05AD934	1	316	56	77	--
Oldman River @ Brocket	OMR1	05AA024	1	581	575	147	32
Oldman River U/S Lethbridge	OMR2	05AD007	1	642	635	249	72
Pincher Creek	PCR	--	--	--	--	--	--
St. Mary River	SMR	05AE006	2	581	575	47	15
Willow Creek	WK	05AB046	0	590	124	18	--
Little Bow River	LBR4	05AC023	0	555	1	8	--
Oldman River @ Taber	OMR3	05AG006	11	642	635	265	78
Expanse Coulee	EC	05AG003	1	555	1	2	--
Ross Creek	RK	--	--	--	--	--	--
Seven Persons Creek	SPC	05AH005	8	642	252	3	--
SSR U/S Medicine Hat	SSR1	--	--	--	--	--	--
SSR D/S Medicine Hat	SSR2	05AJ001	7	642	635	570	244

Table 8: Land use and topography of the sampling sites in the SSRB basin including the percent slope greater and less than 10%, land use (i.e. human footprint) and land cover for areas without a human footprint, with short forms in the table including agriculture (Ag.), oil and gas (O&G), and linear transportation (L. Trans) .

Site Name	ID	Slope (%)		Land Use (%)							Natural Land Cover (%)						
		<10	>10	Ag.	Forestry	Mining	O&G	L.Trans.	Urban	Wetland	Water	Ice	Rock	Exposed	Shurb	Grass	Forest
Bow River @ Cochrane	BR1	26	74	4	2	0	0	1	1	0	3	1	27	0.1	7	8	45
Bow River D/S Carseland Dam	BR2	43	57	16	2	0	0	3	5	1	2	1	16	0.1	7	10	37
Elbow River	ER	41	59	12	3	0	0	4	6	0	2	0	19	0.1	5	8	42
Fish Creek	FC	66	34	24	3	0	0	6	8	0	1	0	0	0.0	4	8	44
Highwood River	HR	42	58	21	2	0	0	2	3	1	1	0	6	0.1	10	13	41
Nose Creek	NC	94	6	48	0	1	0	10	19	2	1	0	0	0.0	0	17	1
Pine Creek	PC	75	25	46	0	0	0	8	14	3	1	0	0	0.1	2	12	12
Bow River @ Cluny	BR3	50	50	22	2	0	0	3	5	1	2	1	14	0.1	6	11	32
East Arrowwood Creek	EAC	97	3	79	0	0	1	3	1	3	0	0	0	0.0	3	10	0
West Arrowwood Creek	WAC	99	1	82	0	0	1	3	1	2	0	0	0	0.0	1	9	0
Bow River @ Ronalane Bridge	BR4	63	37	28	1	0	1	3	4	2	3	0	10	0.1	4	19	23
Coal Creek	CC	100	0	55	0	0	3	2	1	3	0	0	0	0.0	0	35	0
Crowfoot Creek	CFC	97	3	78	0	0	2	3	1	2	1	0	0	0.2	1	10	1
New West Coulee	NWC	100	0	71	0	0	1	3	1	7	1	0	0	0.0	0	15	1
Twelve Mile Creek	TMC	99	1	26	0	0	7	3	1	7	5	0	0	0.1	0	50	0
Beaver Creek	BRC	34	66	17	5	0	0	1	0	2	0	0	0	0.1	9	42	22
Belly River	BYR	67	33	36	0	0	0	2	1	3	4	0	7	1.1	6	21	20
Oldman River @ Brocket	OMR1	25	75	9	9	0	0	1	1	1	1	0	5	0.2	13	16	43
Oldman River U/S Lethbridge	OMR2	56	44	30	3	0	0	2	1	2	3	0	4	0.6	8	23	23
Pincher Creek	PRC	72	28	45	1	0	0	3	3	3	1	0	2	0.1	5	19	18
St. Mary River	SMR	65	35	35	1	0	0	2	1	2	4	0	4	1.3	7	26	17
Willow Creek	WK	51	49	26	1	0	0	2	1	2	1	0	0	0.1	11	35	20
Little Bow River	LBR	95	5	72	0	0	1	3	1	4	2	0	0	0.2	1	15	0
Oldman River @ Taber	OMR3	68	32	44	2	0	0	2	2	2	3	0	3	0.5	6	20	16
Expanse Coulee	EC	100	0	68	0	0	2	3	1	4	3	0	0	0.0	0	19	0
Ross Creek	RK	86	14	37	0	0	1	2	2	2	4	0	0	0.1	3	43	5
Seven Persons Creek	SPC	94	6	59	0	0	1	2	2	3	2	0	0	0.2	0	31	0
SSR U/S Medicine Hat	SSR1	69	31	39	1	0	1	3	3	2	3	0	6	0.3	5	20	17
SSR D/S Medicine Hat	SSR2	71	29	40	1	0	1	3	2	2	3	0	5	0.3	4	21	16

Figure 2: The confidence interval (CI) (i.e. +/- 150%) for total recoverable metals (left) and dissolved metals (right) that were modelled (black) or were not modelled (red) based on the analyses of the duplicate quality control samples for all percentiles of environmental data sampled by the Calgary field office.

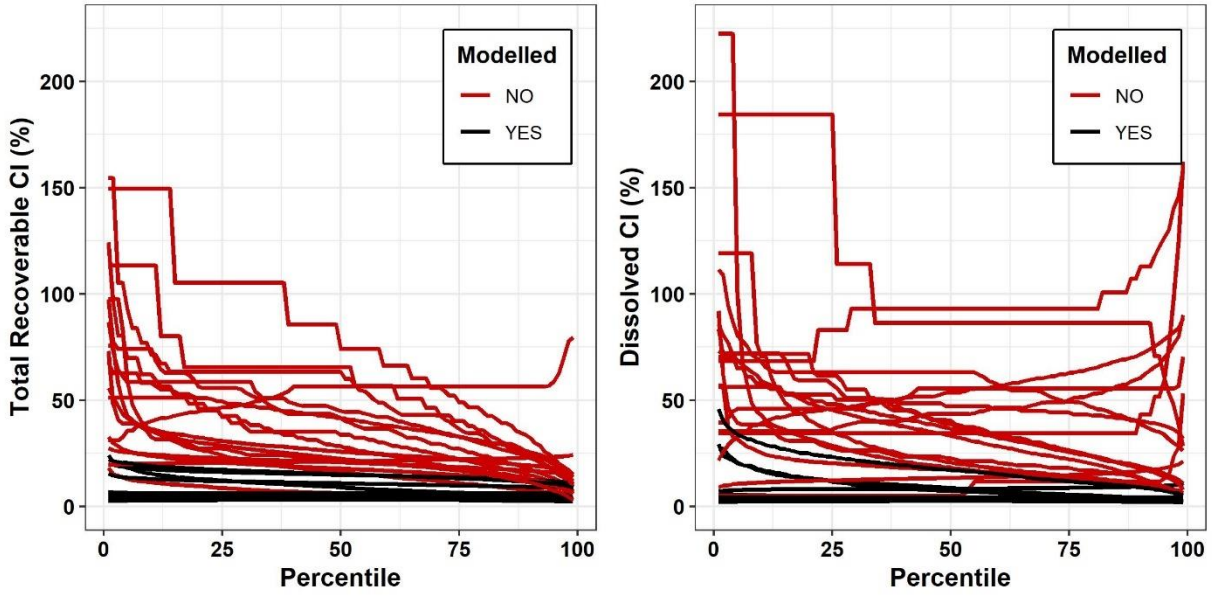

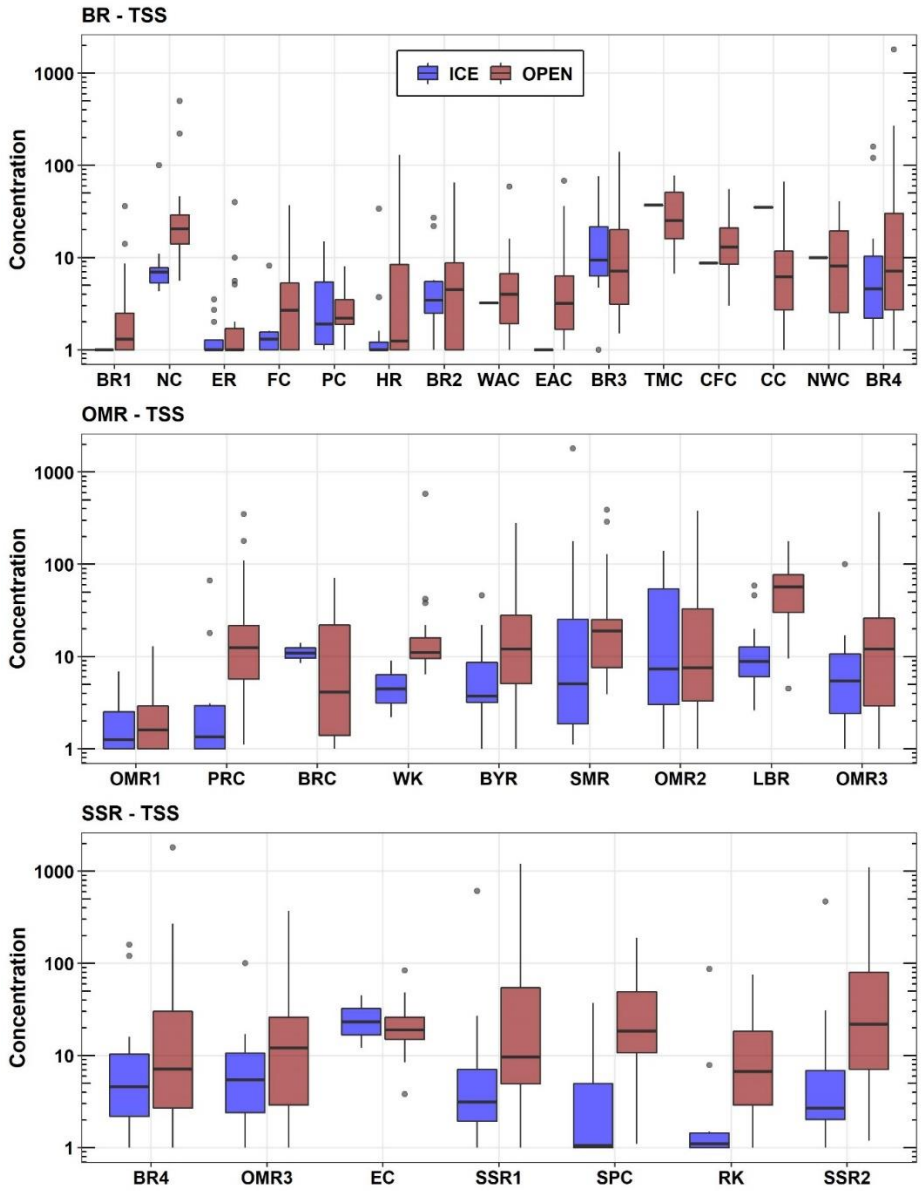

Figure 3: Total suspended sediment (TSS) concentrations for the Bow (BR), Oldman (OMR) and South Saskatchewan River (SSR) systems for the ice-covered (blue – November to March) and open water (red – April to October) seasons. Of note it is often not possible to sample all sites in the winter.

0

Supplementary Information

Figure S1: Discharge in cubic metres per second (cms) for mainstem sites where streamflow data was available streamflow for the sampling dates.

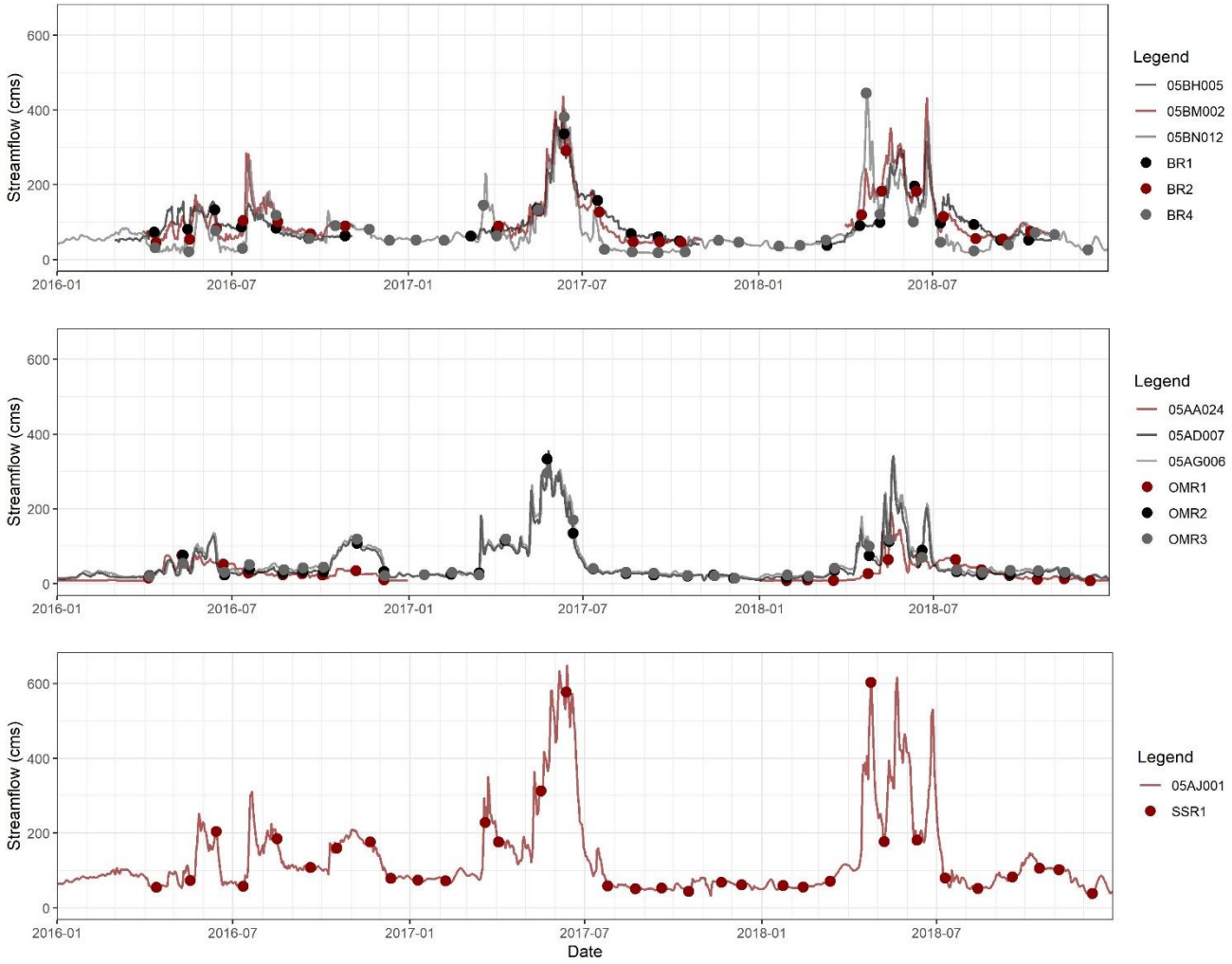

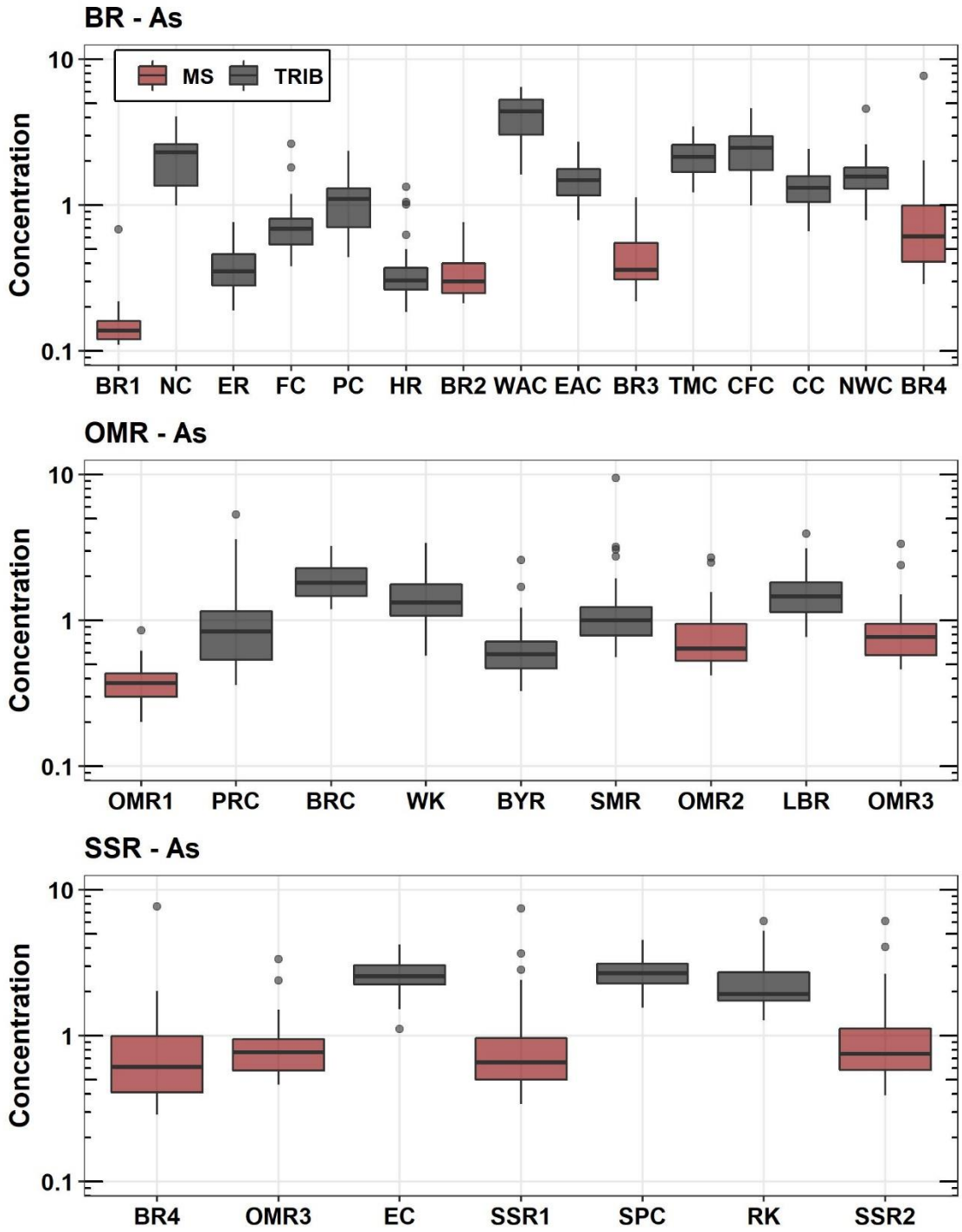

Figure S2: Box plots of the modelled total recoverable Arsenic (As) concentrations for the Bow River (BR – Top), Oldman River (OMR – middle) and South Saskatchewan River (SSR) including main stem (MS – red)) and tributary (TRIB – grey) sites for all annual samples.

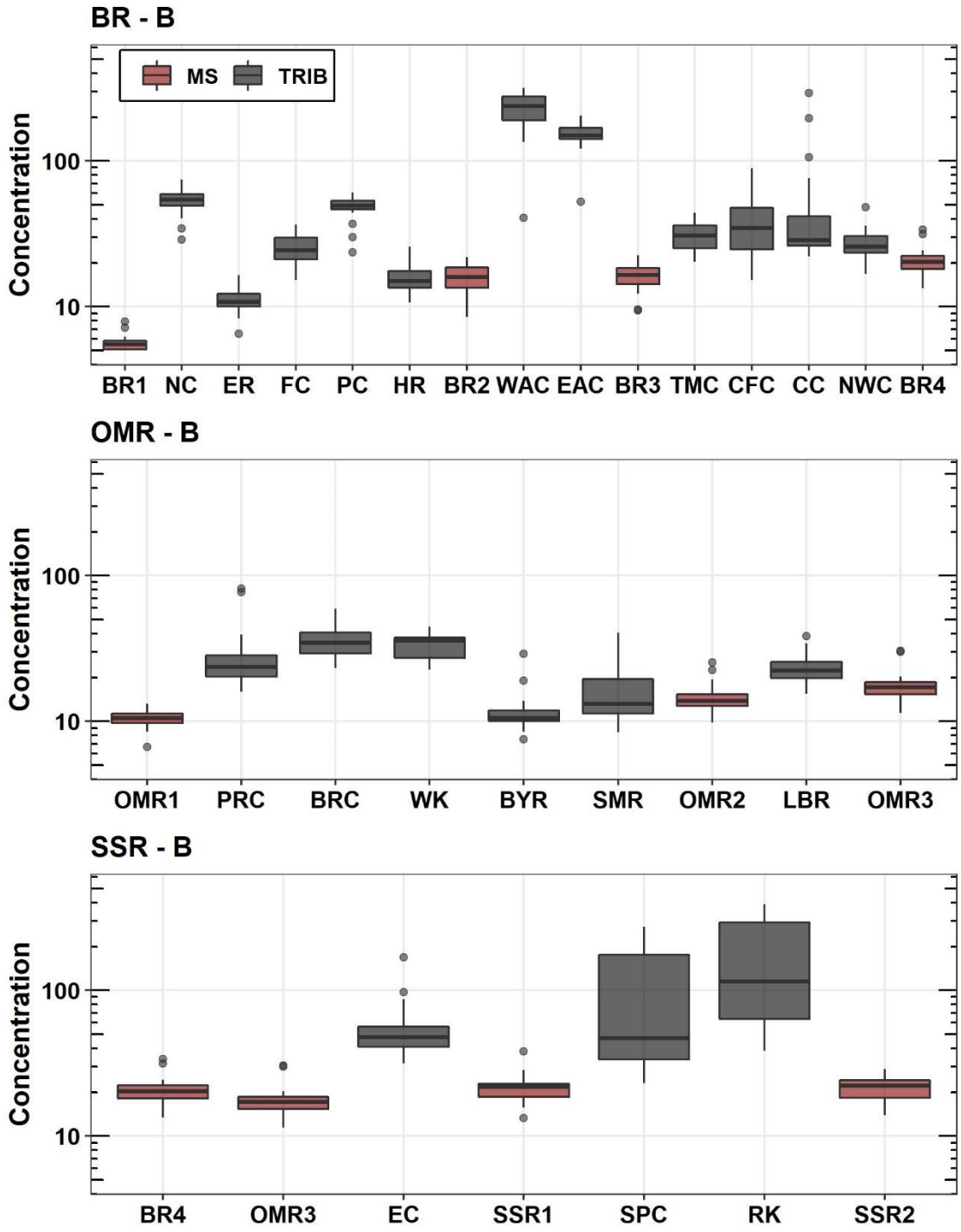

Figure S3: Box plots of the modelled total recoverable Boron (B) concentrations for the Bow River (BR – Top), Oldman River (OMR – middle) and South Saskatchewan River (SSR) including main stem (MS – red)) and tributary (TRIB – grey) sites for all annual samples.

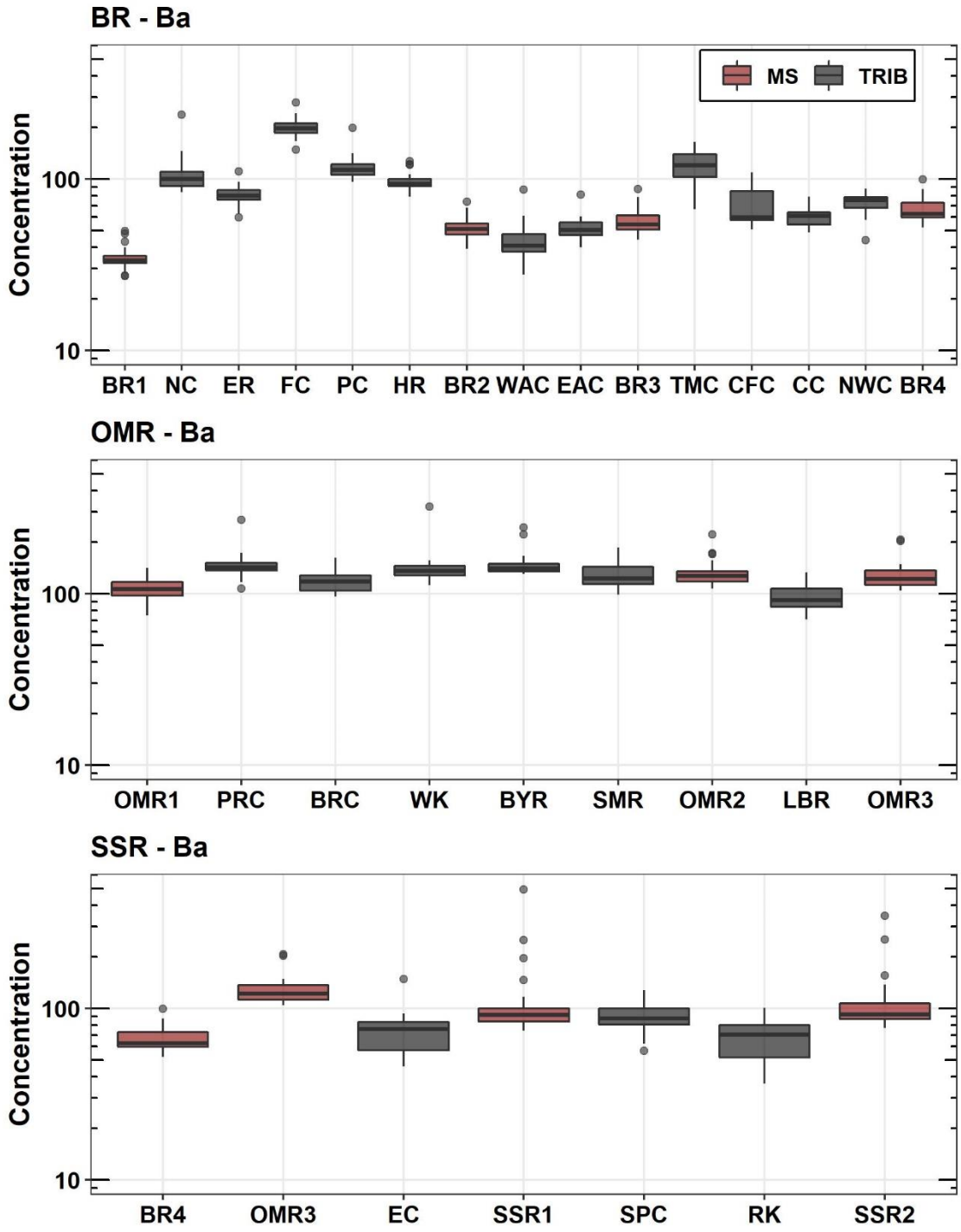

Figure S4: Box plots of the modelled total recoverable Barium (Ba) concentrations for the Bow River (BR – Top), Oldman River (OMR – middle) and South Saskatchewan River (SSR) including main stem (MS – red)) and tributary (TRIB – grey) sites for all annual samples.

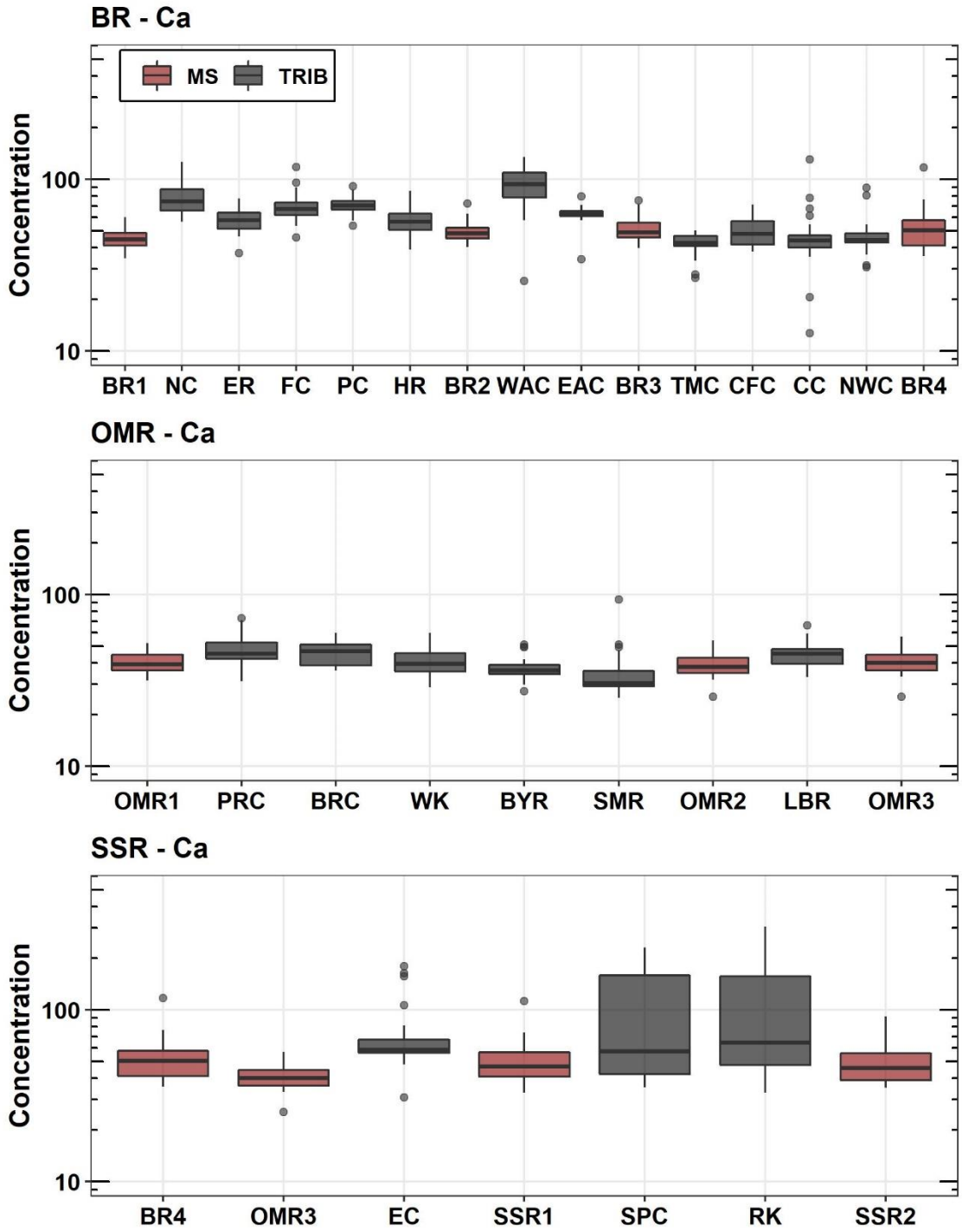

Figure S5: Box plots of the modelled total recoverable Calcium (Ca) concentrations for the Bow River (BR – Top), Oldman River (OMR – middle) and South Saskatchewan River (SSR) including main stem (MS – red)) and tributary (TRIB – grey) sites for all annual samples.

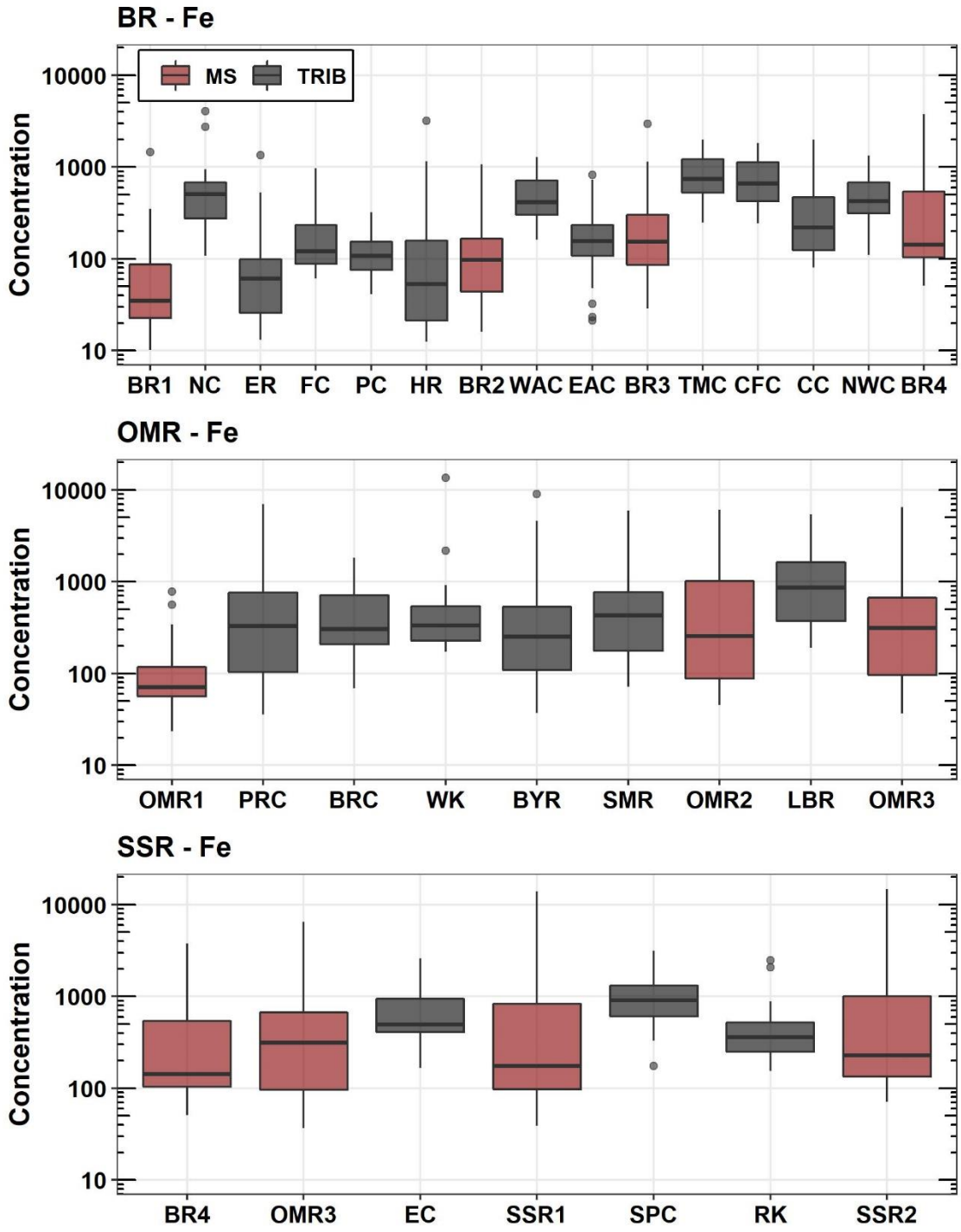

Figure S6: Box plots of the modelled total recoverable Iron (Fe) concentrations for the Bow River (BR – Top), Oldman River (OMR – middle) and South Saskatchewan River (SSR) including main stem (MS – red)) and tributary (TRIB – grey) sites for all annual samples.

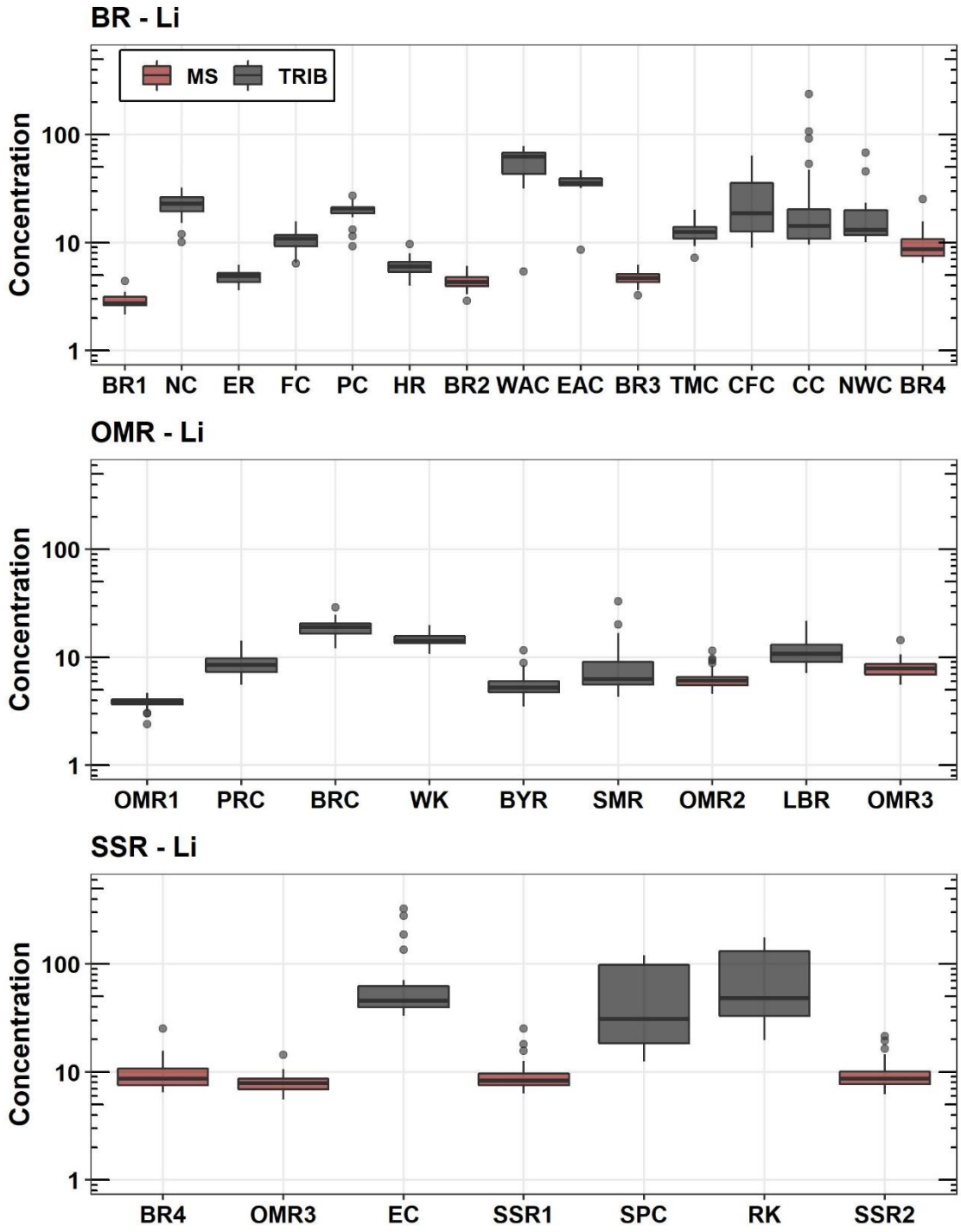

Figure S7: Box plots of the modelled total recoverable Lithium (Li) concentrations for the Bow River (BR – Top), Oldman River (OMR – middle) and South Saskatchewan River (SSR) including main stem (MS – red)) and tributary (TRIB – grey) sites for all annual samples.

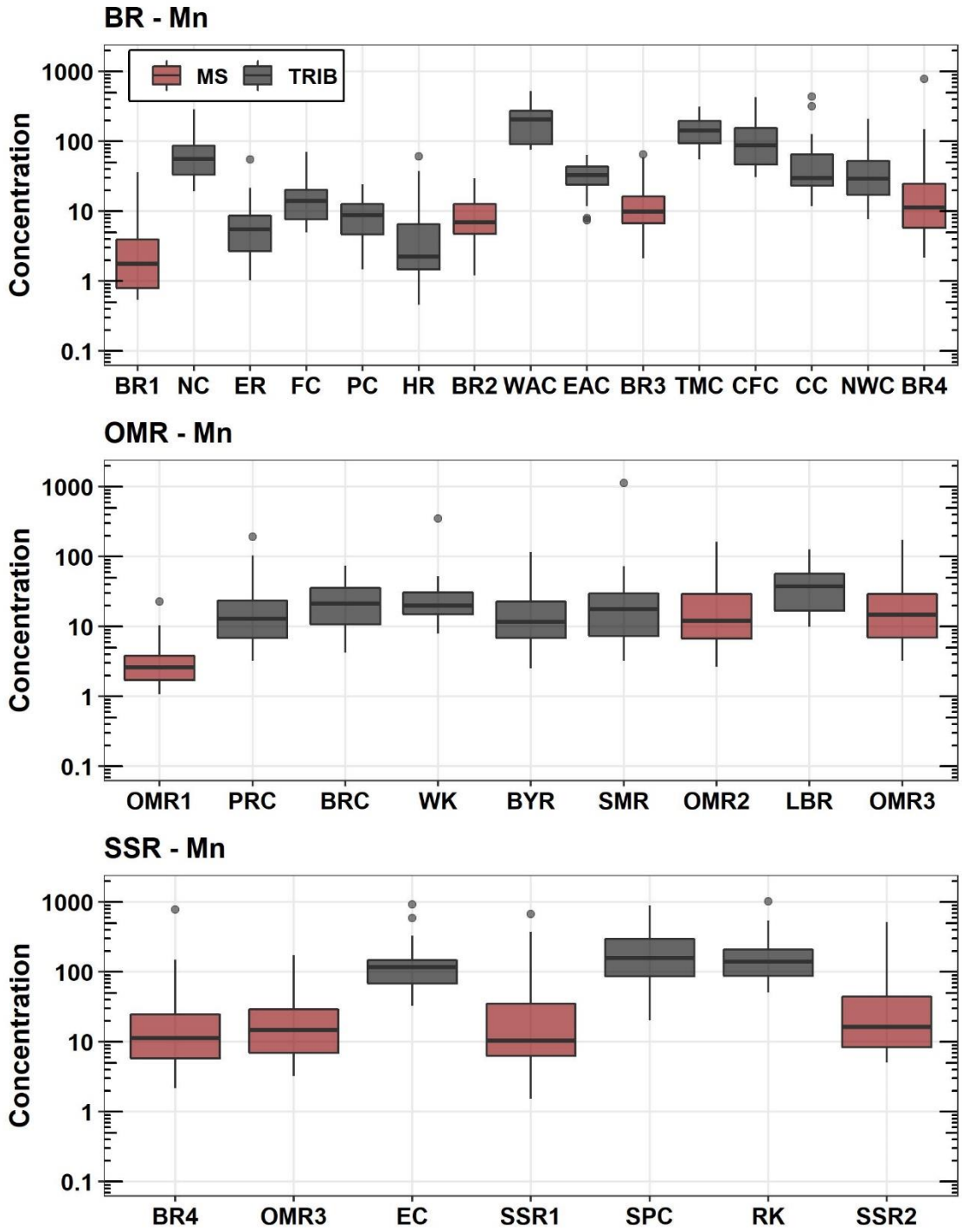

Figure S8: Box plots of the modelled total recoverable Manganese (Mn) concentrations for the Bow River (BR – Top), Oldman River (OMR – middle) and South Saskatchewan River (SSR) including main stem (MS – red)) and tributary (TRIB – grey) sites for all annual samples.

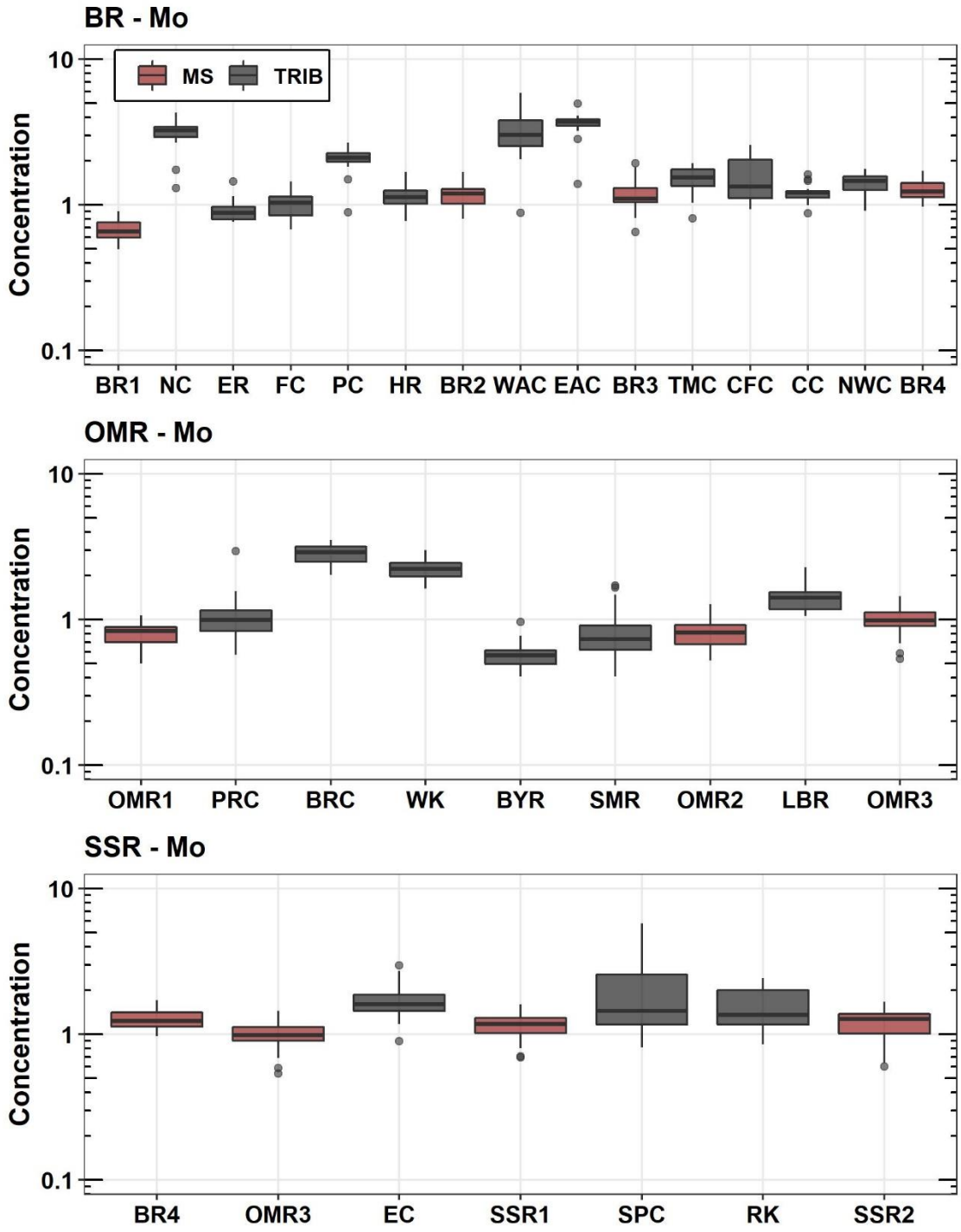

Figure S9: Box plots of the modelled total recoverable Molybdenum (Mo) concentrations for the Bow River (BR – Top), Oldman River (OMR – middle) and South Saskatchewan River (SSR) including main stem (MS – red)) and tributary (TRIB – grey) sites for all annual samples.

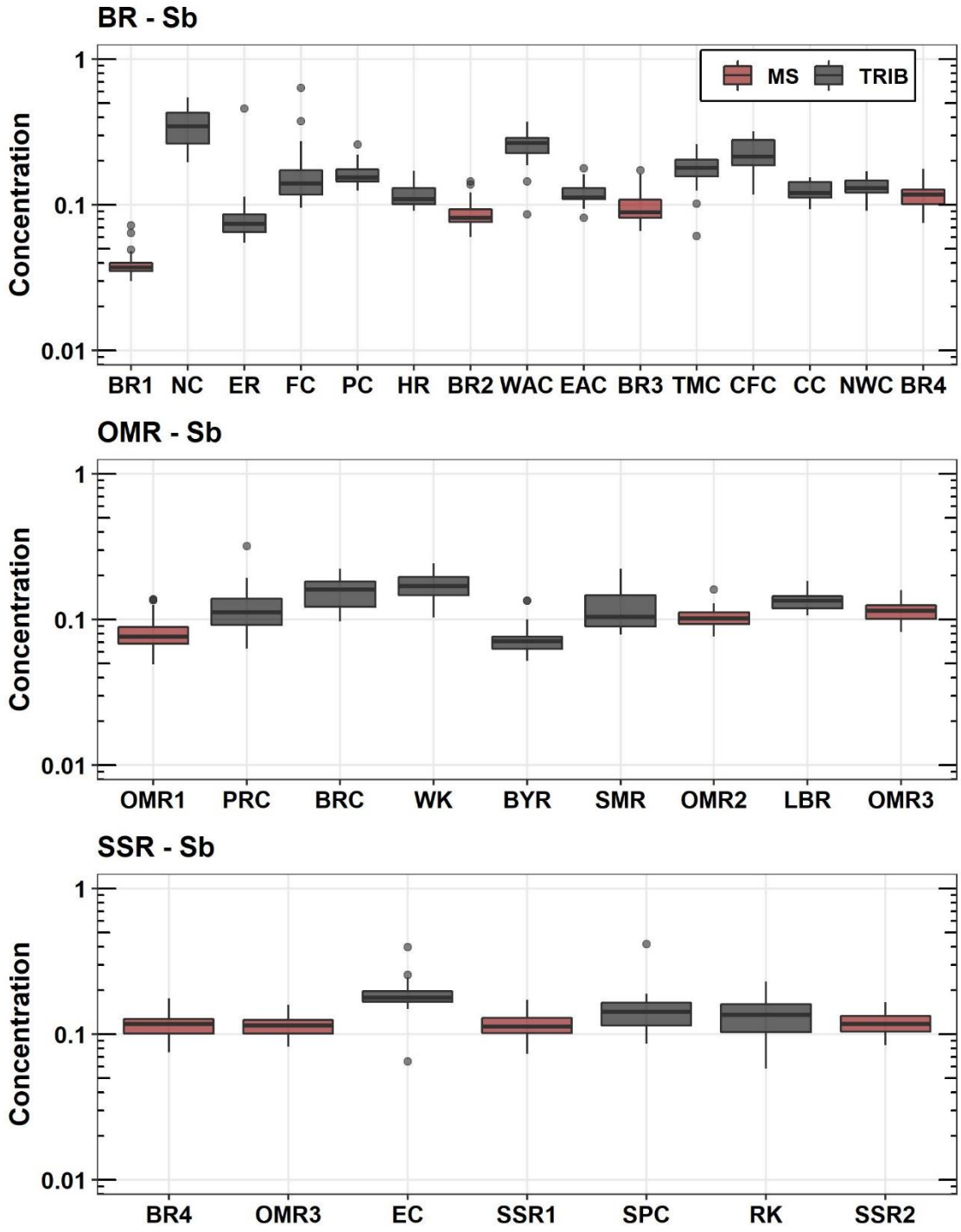

Figure S10: Box plots of the modelled total recoverable Antimony (Sb) concentrations for the Bow River (BR – Top), Oldman River (OMR – middle) and South Saskatchewan River (SSR) including main stem (MS – red)) and tributary (TRIB – grey) sites for all annual samples.

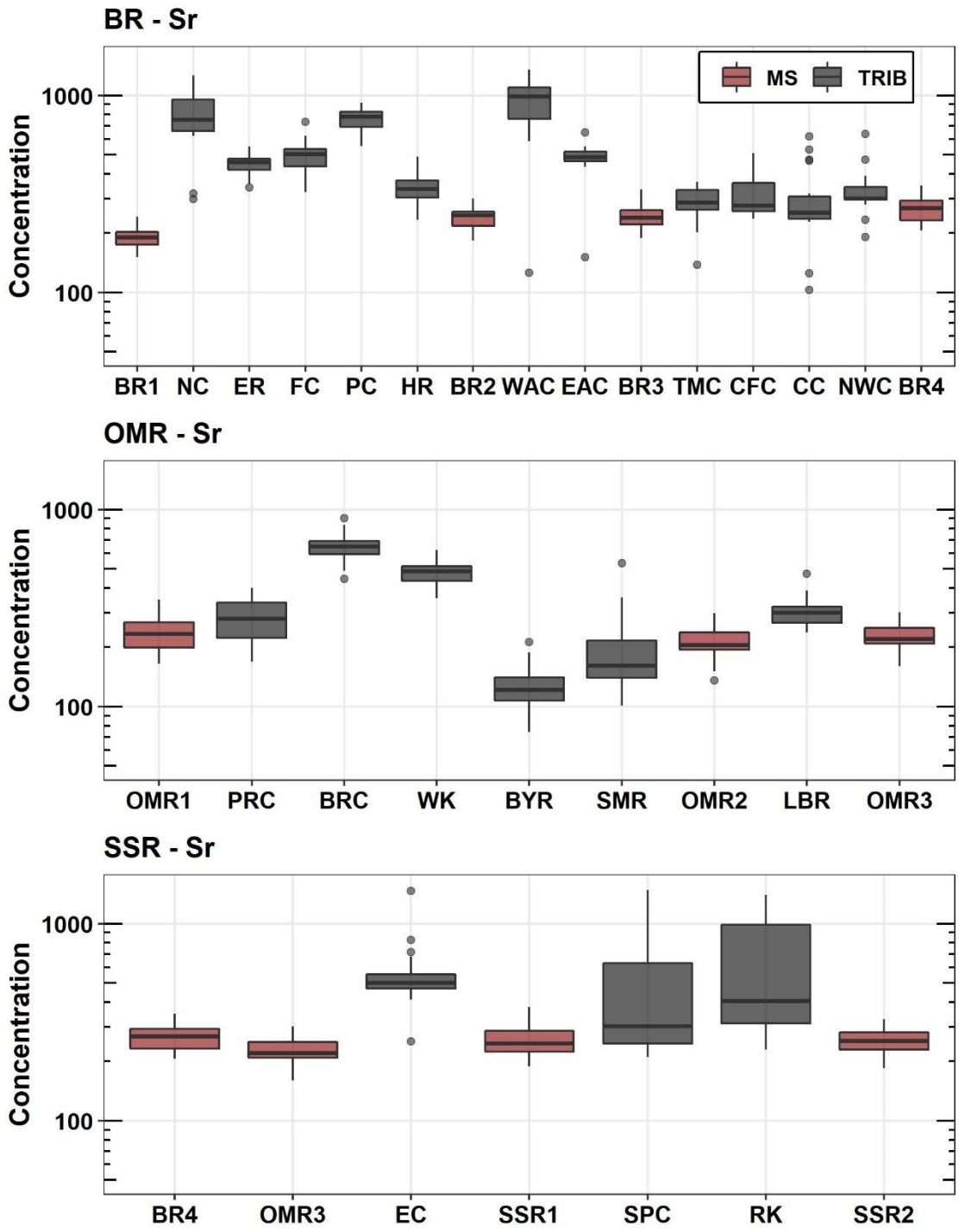

Figure S11: Box plots of the modelled total recoverable Strontium (Sr) concentrations for the Bow River (BR – Top), Oldman River (OMR – middle) and South Saskatchewan River (SSR) including main stem (MS – red)) and tributary (TRIB – grey) sites for all annual samples.

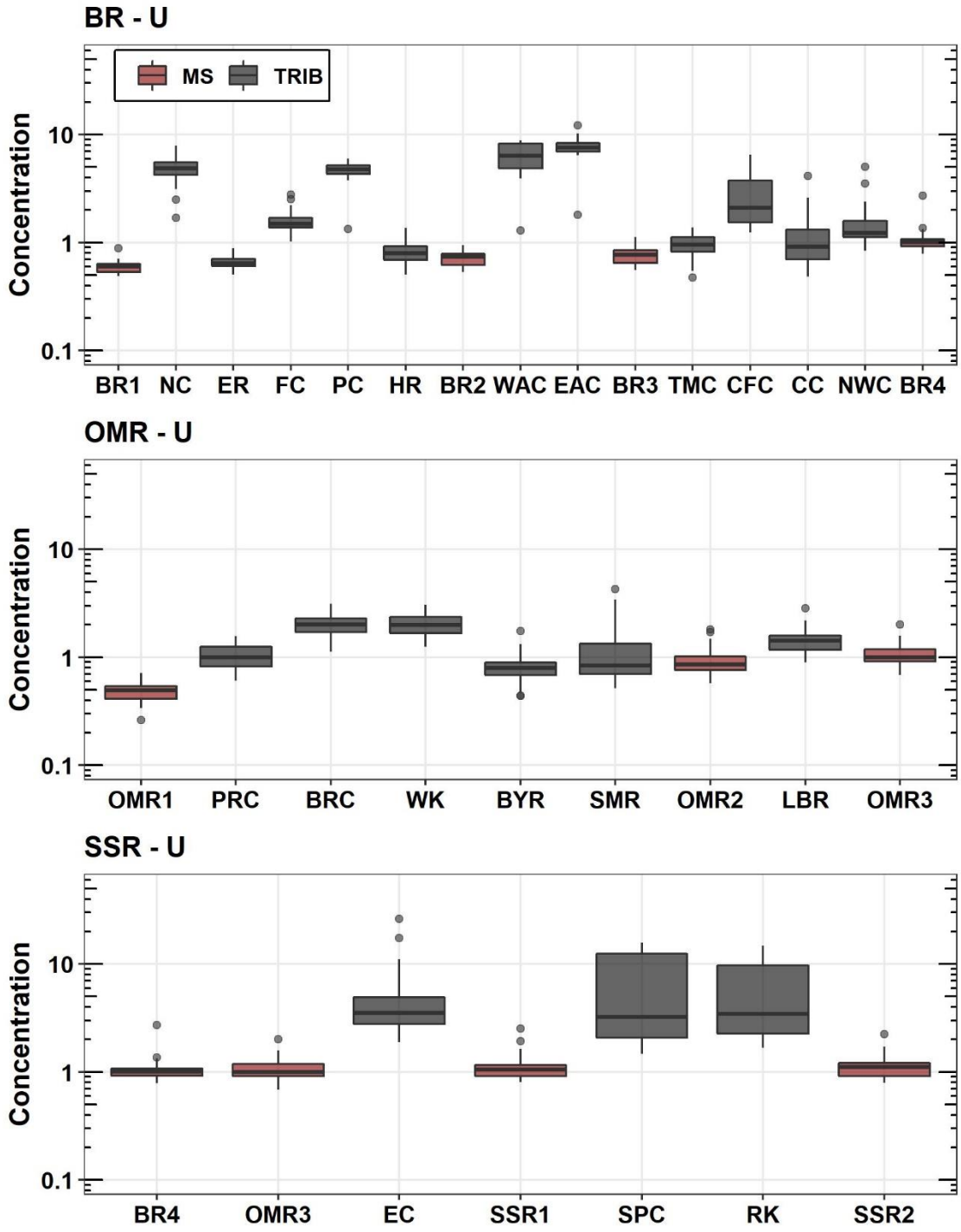

Figure S12: Box plots of the modelled total recoverable Uranium (U) concentrations for the Bow River (BR – Top), Oldman River (OMR – middle) and South Saskatchewan River (SSR) including main stem (MS – red)) and tributary (TRIB – grey) sites for all annual samples.

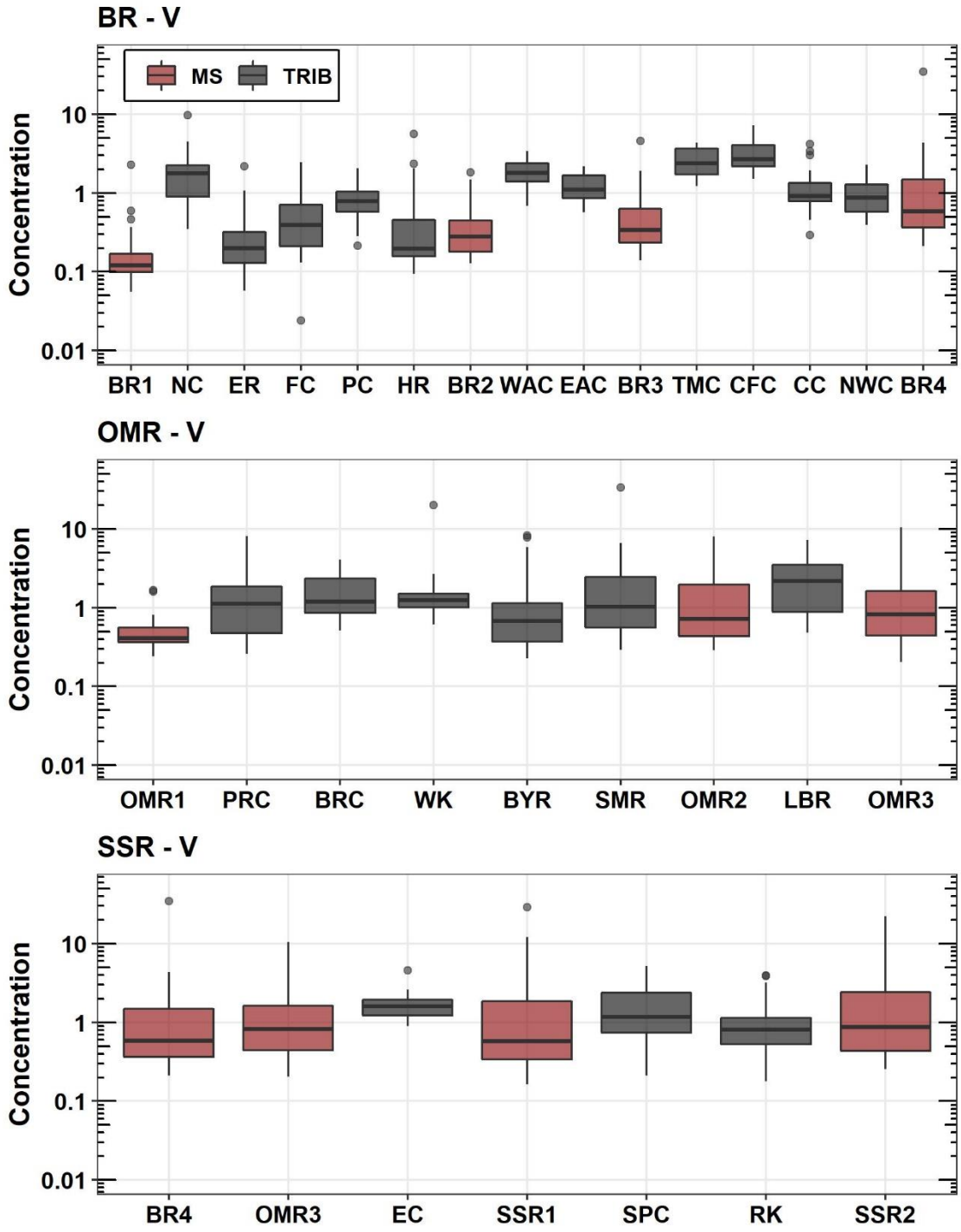

Figure S13: Box plots of the modelled total recoverable Vanadium (V) concentrations for the Bow River (BR – Top), Oldman River (OMR – middle) and South Saskatchewan River (SSR) including main stem (MS – red)) and tributary (TRIB – grey) sites for all annual samples.

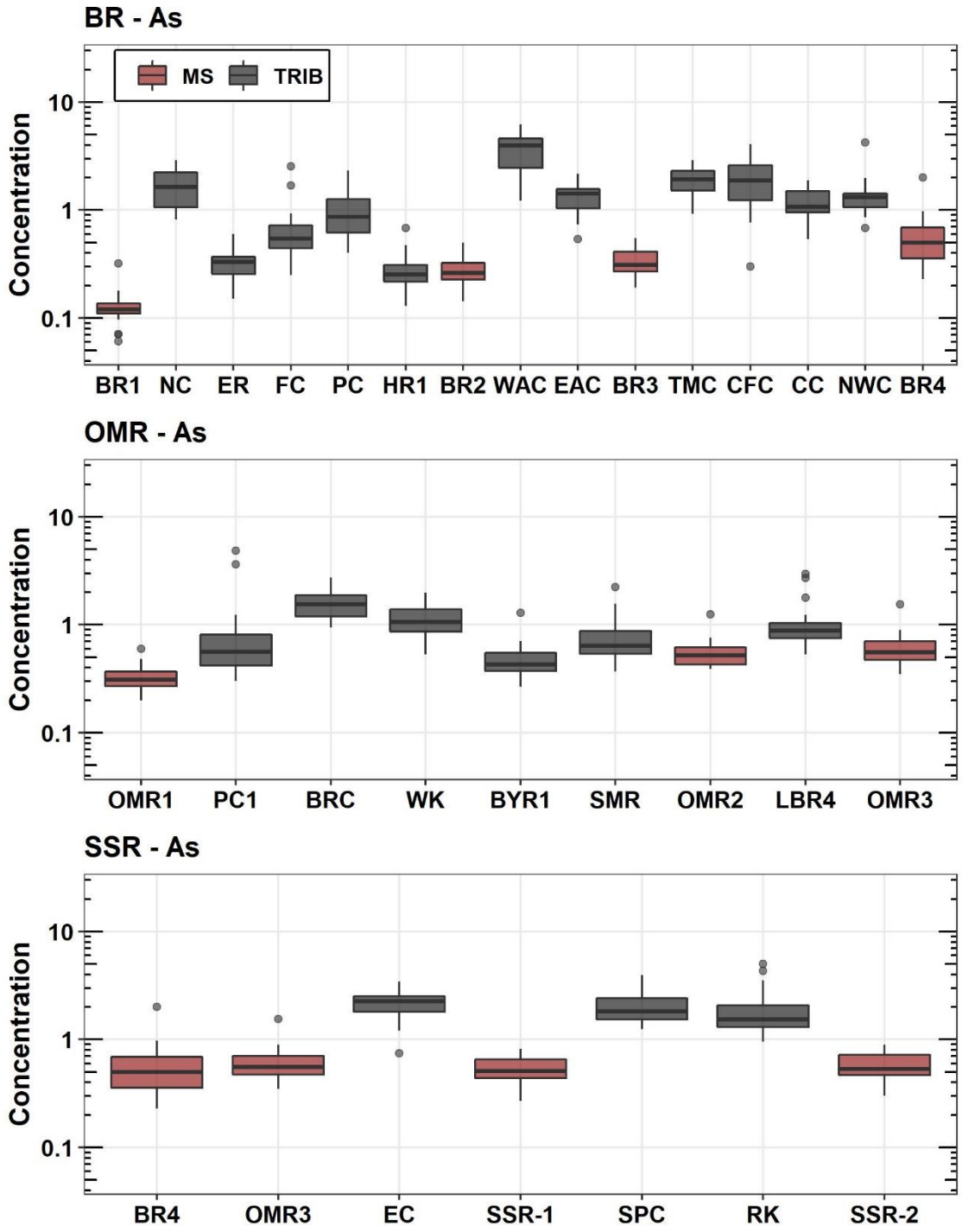

Figure S14: Box plots of the modelled dissolved Arsenic (As) concentrations for the Bow River (BR – Top), Oldman River (OMR – middle) and South Saskatchewan River (SSR) including main stem (MS – red)) and tributary (TRIB – grey) sites for all annual samples.

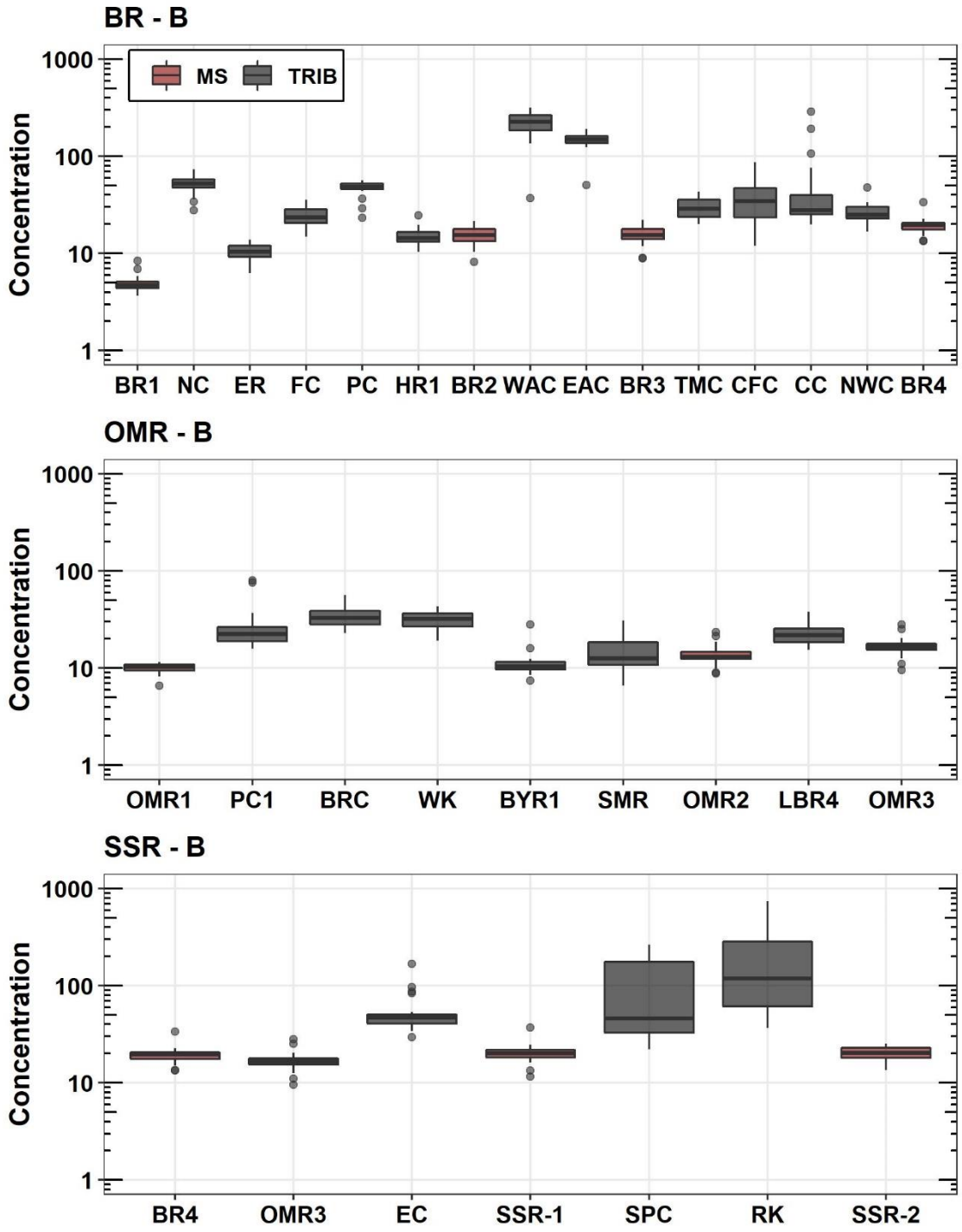

Figure S15: Box plots of the modelled dissolved Boron (B) concentrations for the Bow River (BR – Top), Oldman River (OMR – middle) and South Saskatchewan River (SSR) including main stem (MS – red)) and tributary (TRIB – grey) sites for all annual samples.

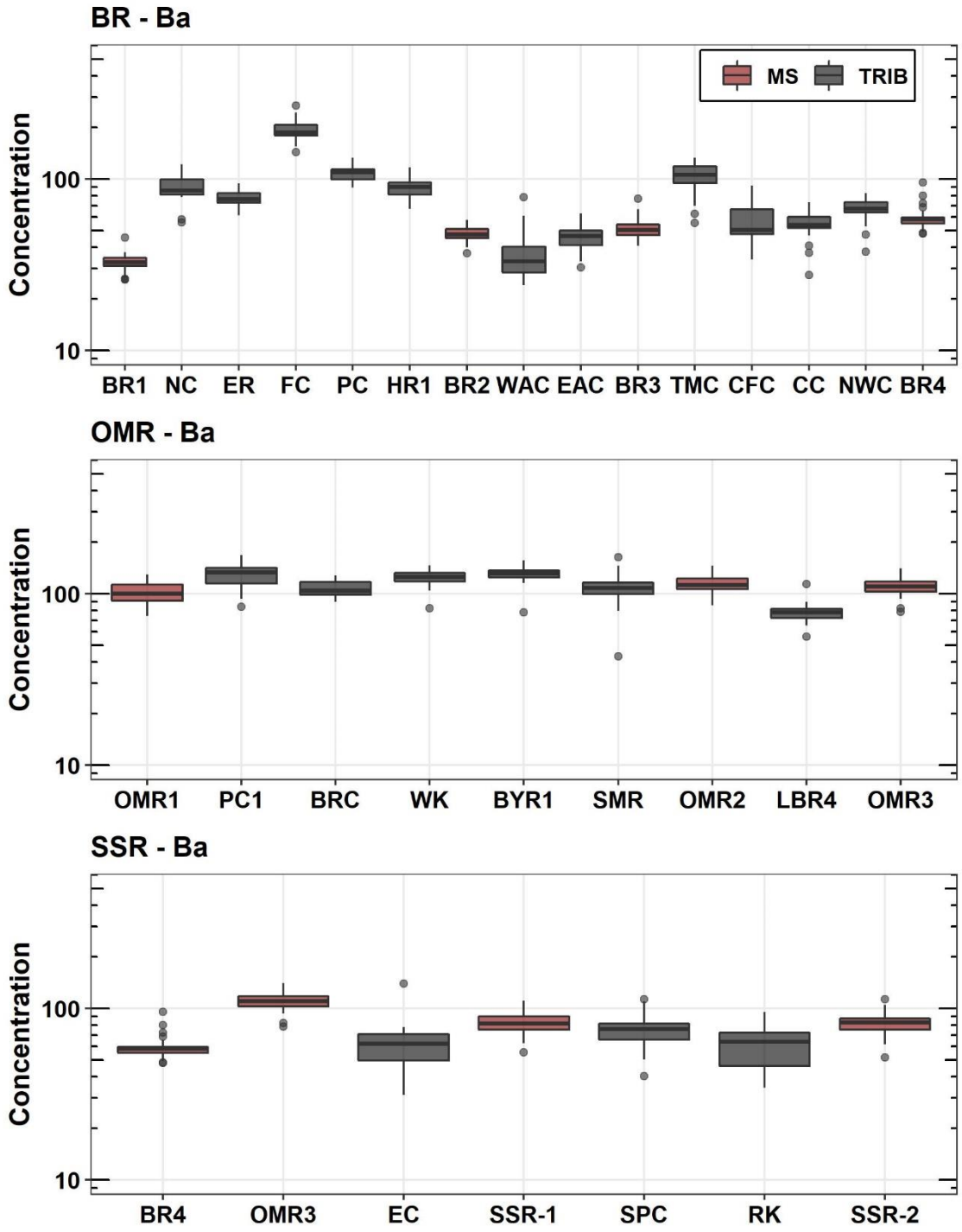

Figure S16: Box plots of the modelled dissolved Barium (Ba) concentrations for the Bow River (BR – Top), Oldman River (OMR – middle) and South Saskatchewan River (SSR) including main stem (MS – red)) and tributary (TRIB – grey) sites for all annual samples.

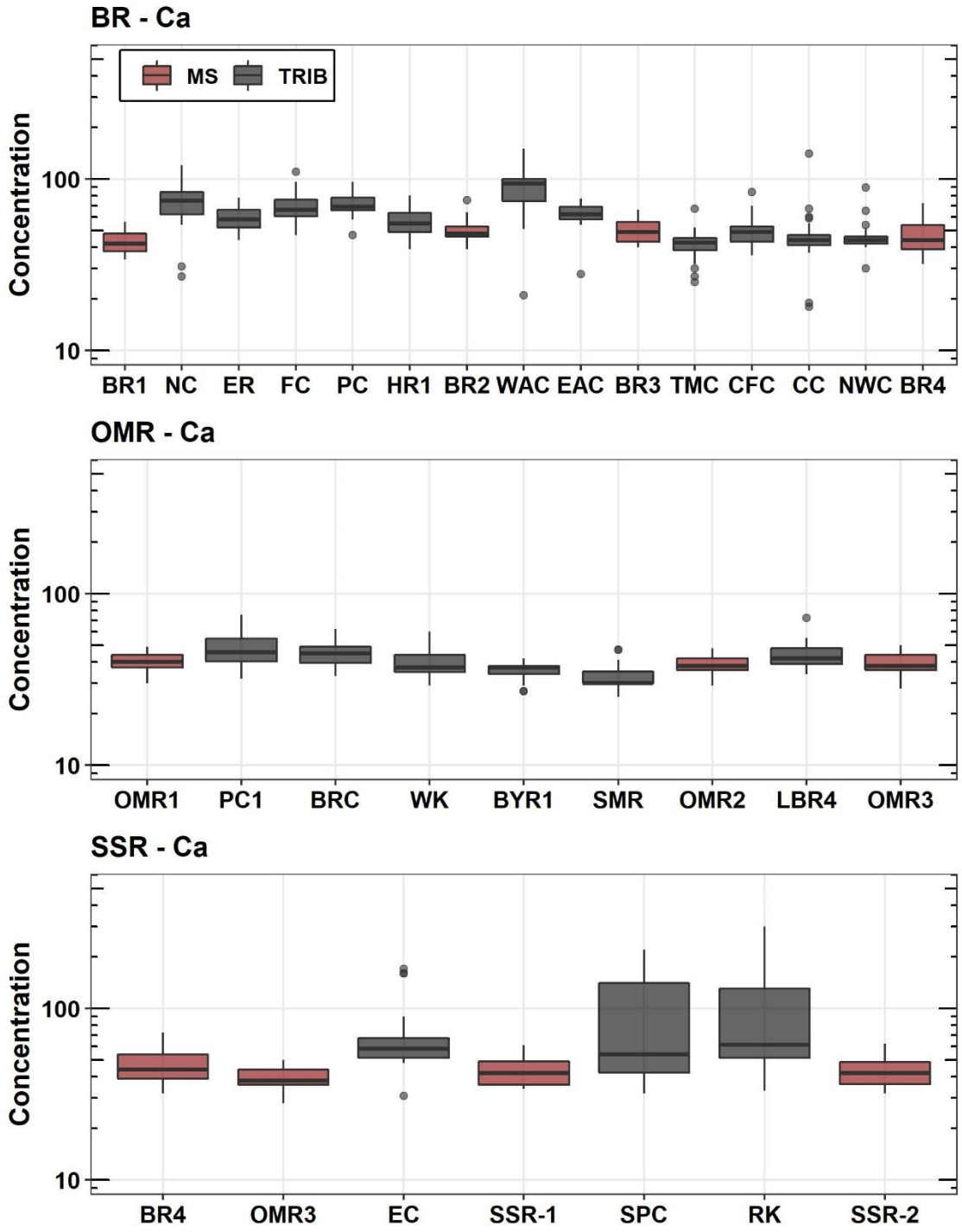

Figure S17: Box plots of the modelled dissolved Calcium (Ca) concentrations for the Bow River (BR – Top), Oldman River (OMR – middle) and South Saskatchewan River (SSR) including main stem (MS – red)) and tributary (TRIB – grey) sites for all annual samples.

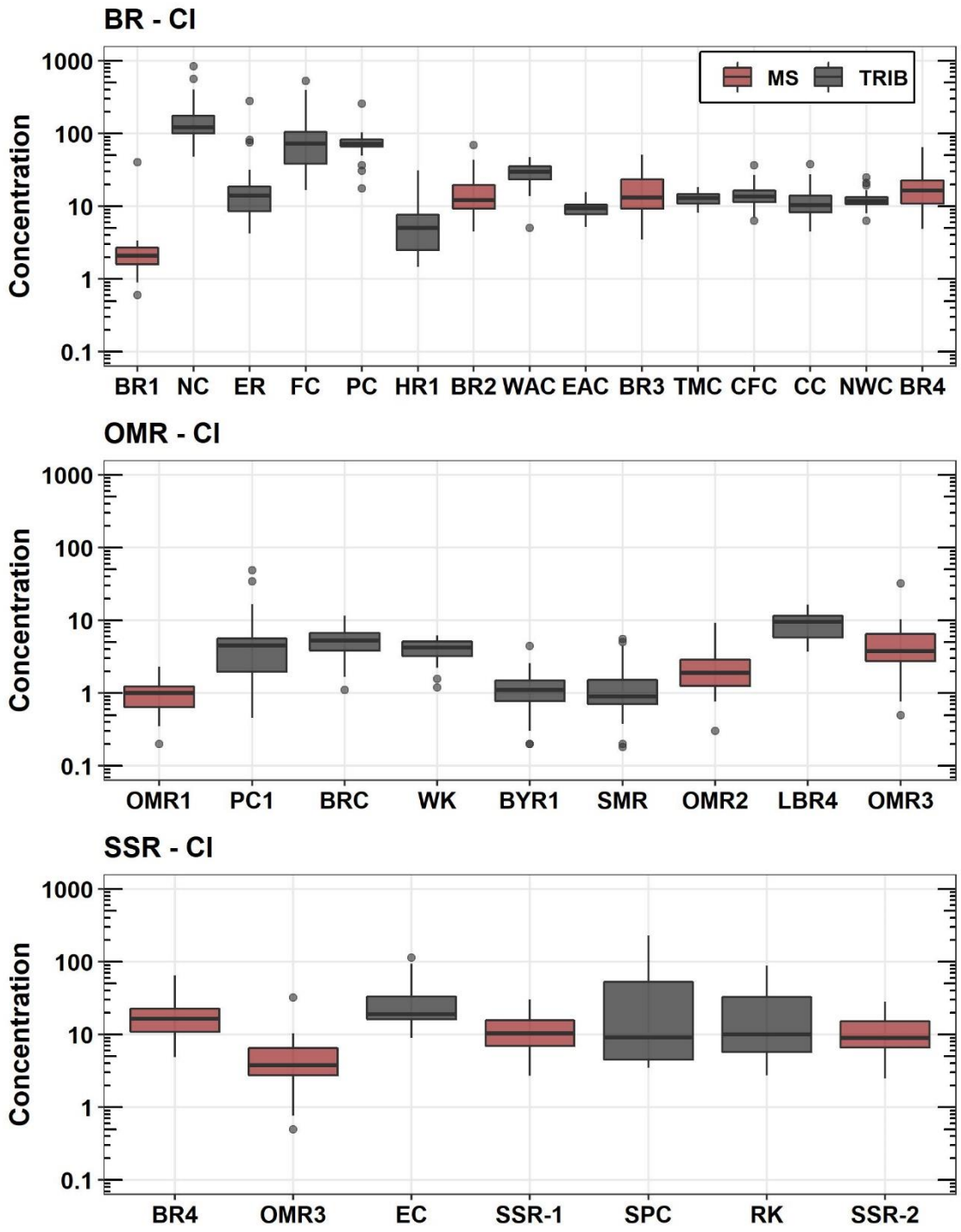

Figure S18: Box plots of the modelled dissolved Chloride (Cl) concentrations for the Bow River (BR – Top), Oldman River (OMR – middle) and South Saskatchewan River (SSR) including main stem (MS – red)) and tributary (TRIB – grey) sites for all annual samples.

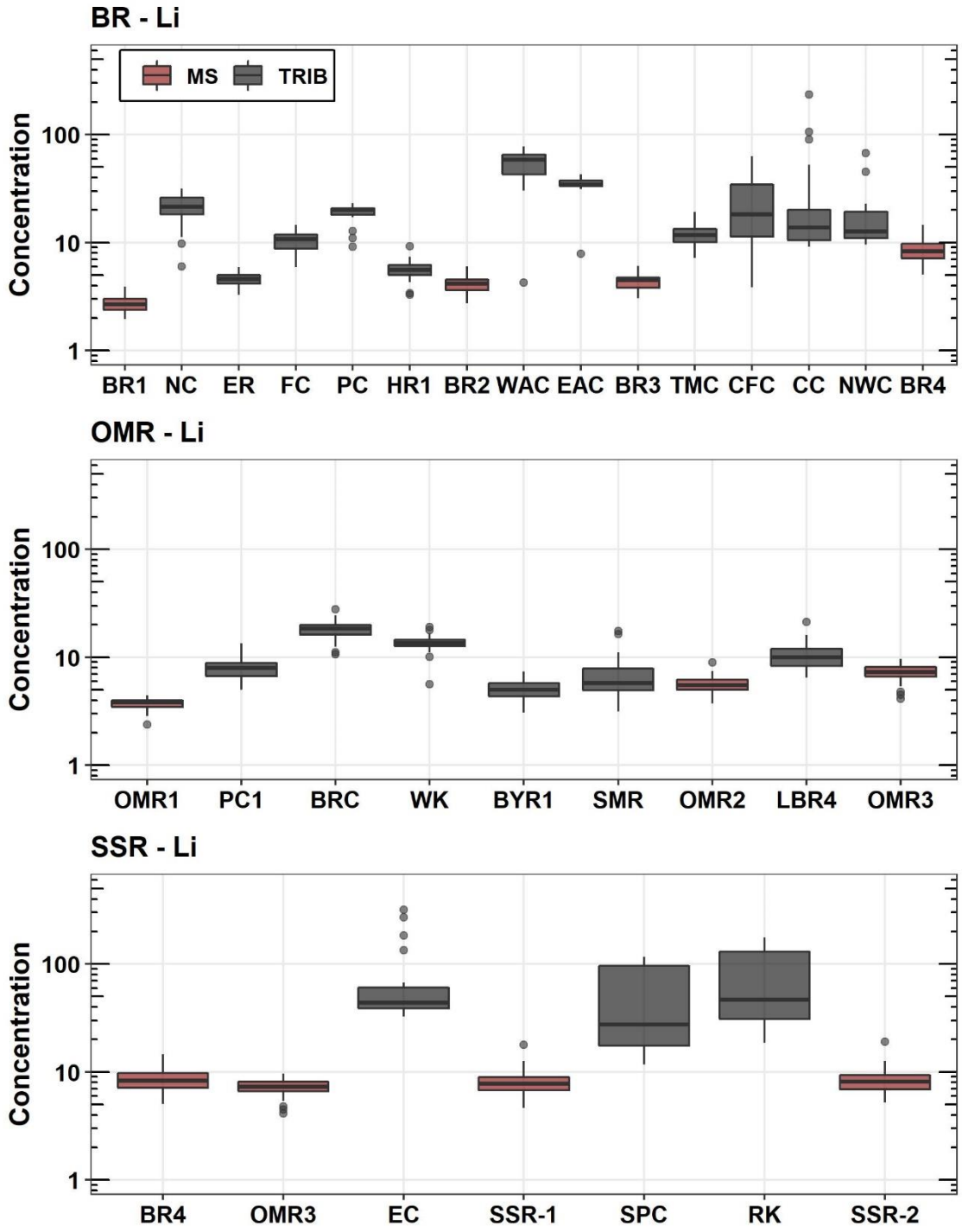

Figure S19: Box plots of the modelled dissolved Lithium (Li) concentrations for the Bow River (BR – Top), Oldman River (OMR – middle) and South Saskatchewan River (SSR) including main stem (MS – red)) and tributary (TRIB – grey) sites for all annual samples.

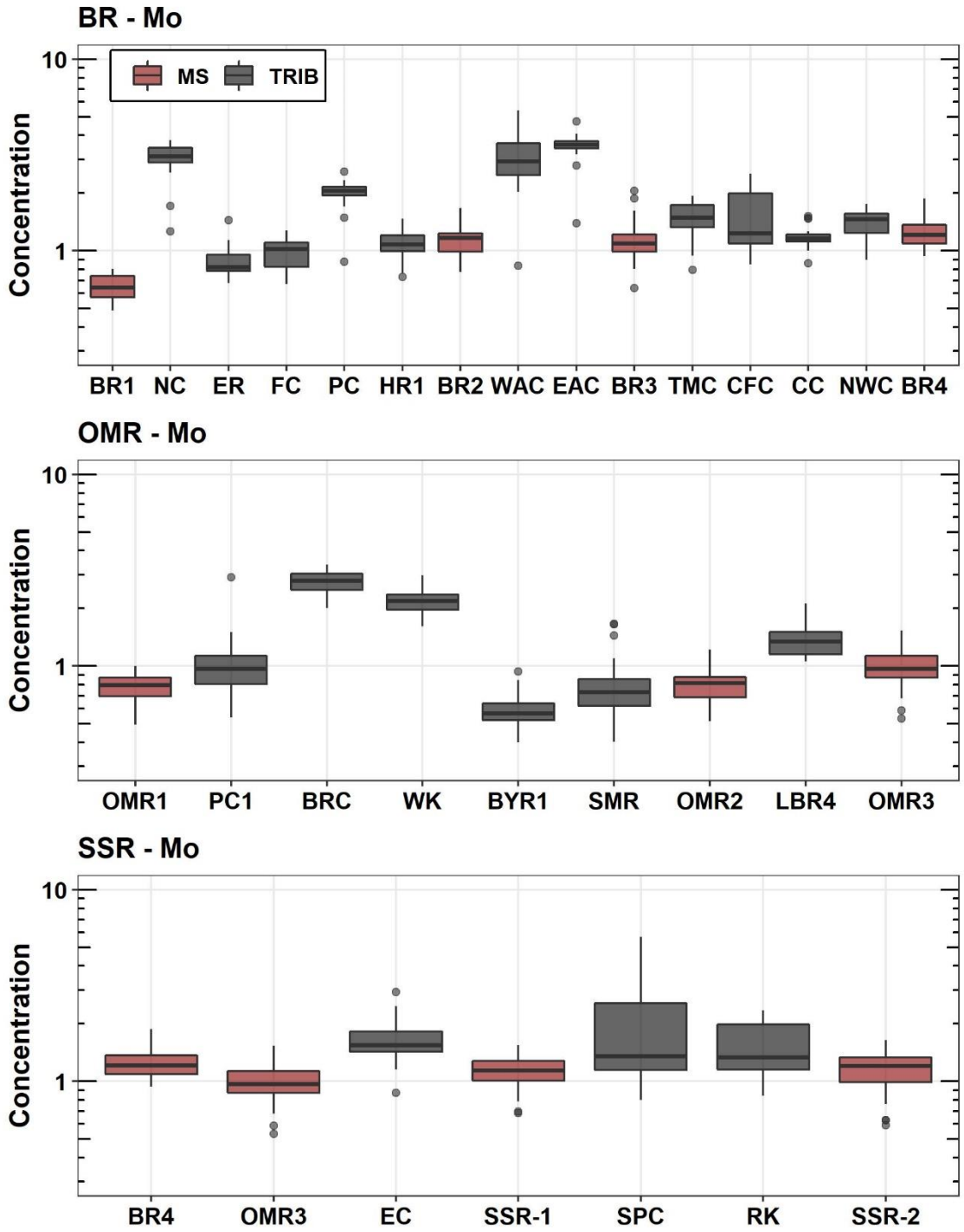

Figure S20: Box plots of the modelled dissolved Molybdenum (Mo) concentrations for the Bow River (BR – Top), Oldman River (OMR – middle) and South Saskatchewan River (SSR) including main stem (MS – red)) and tributary (TRIB – grey) sites for all annual samples.

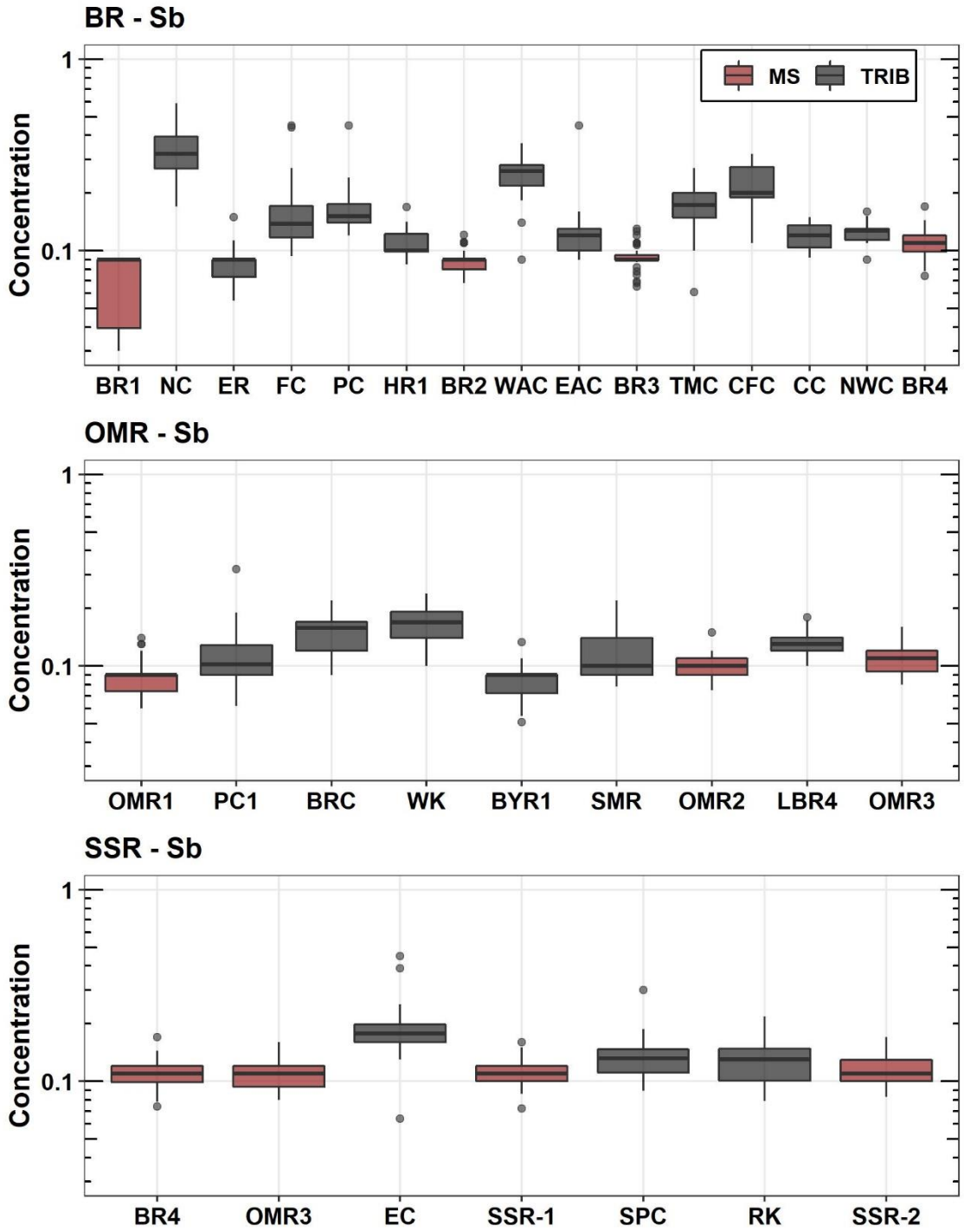

Figure S21: Box plots of the modelled dissolved Antimony (Sb) concentrations for the Bow River (BR – Top), Oldman River (OMR – middle) and South Saskatchewan River (SSR) including main stem (MS – red)) and tributary (TRIB – grey) sites for all annual samples.

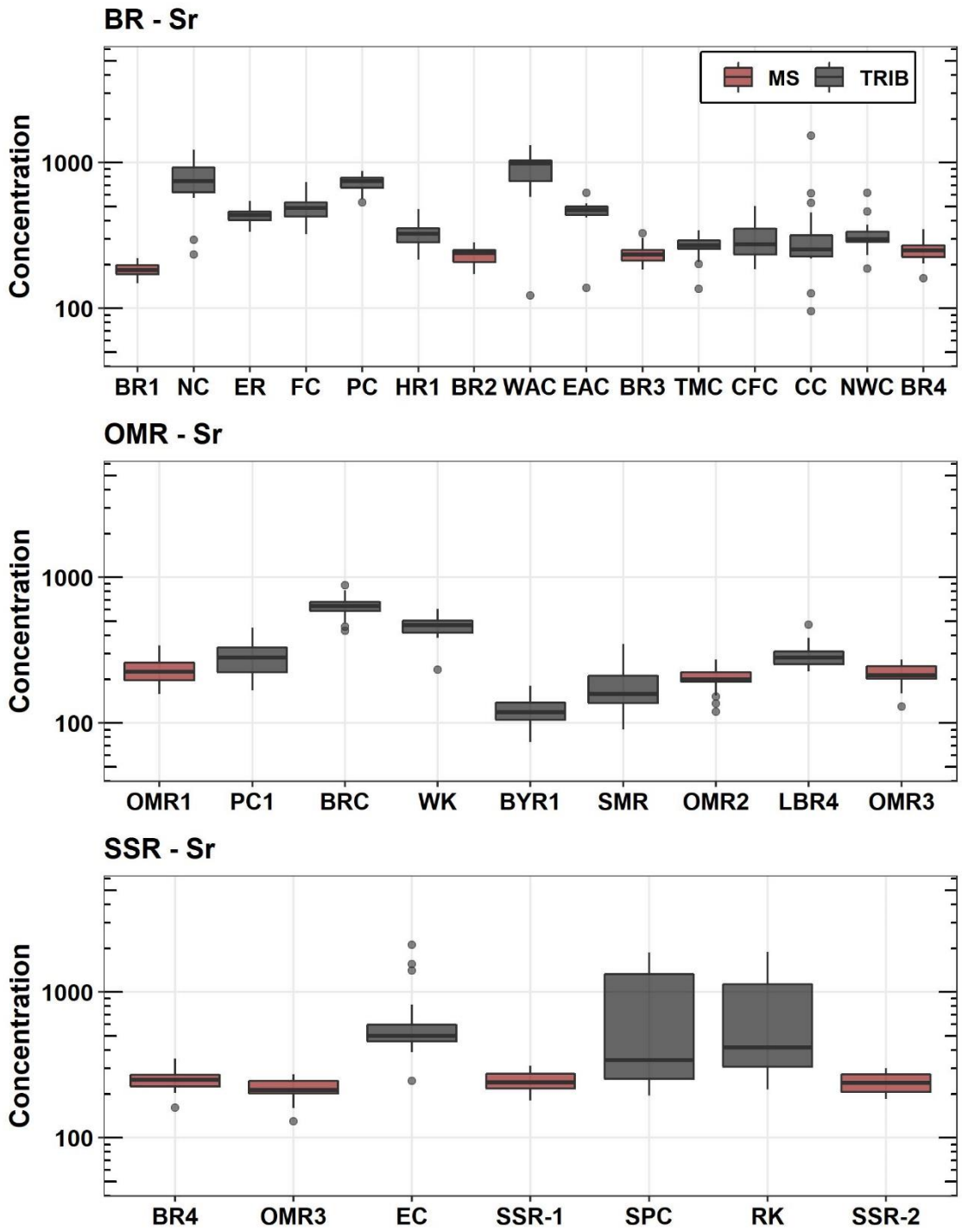

Figure S22: Box plots of the modelled dissolved Strontium (Sr) concentrations for the Bow River (BR – Top), Oldman River (OMR – middle) and South Saskatchewan River (SSR) including main stem (MS – red)) and tributary (TRIB – grey) sites for all annual samples.

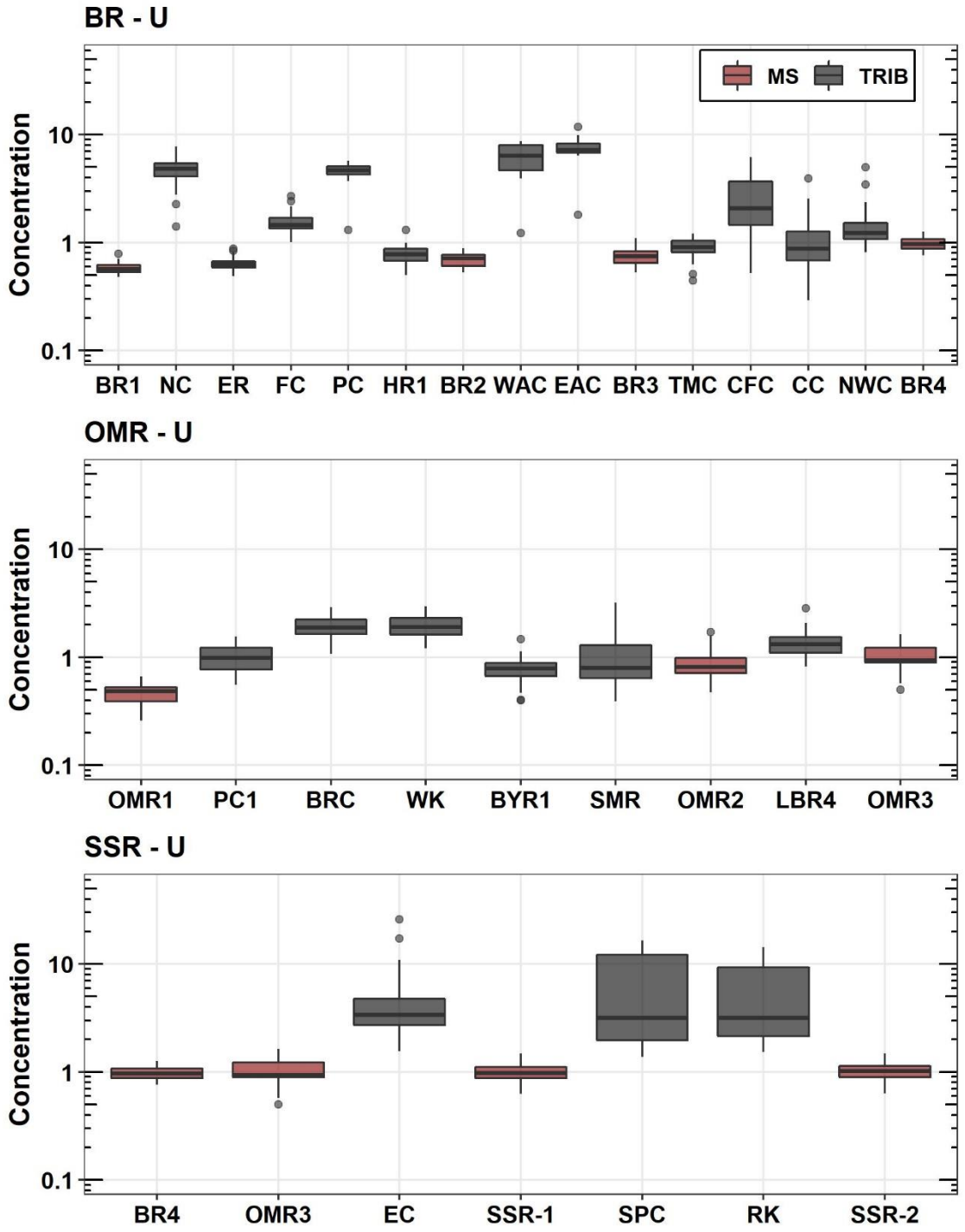

Figure S23: Box plots of the modelled dissolved Uranium (U) concentrations for the Bow River (BR – Top), Oldman River (OMR – middle) and South Saskatchewan River (SSR) including main stem (MS – red)) and tributary (TRIB – grey) sites for all annual samples.

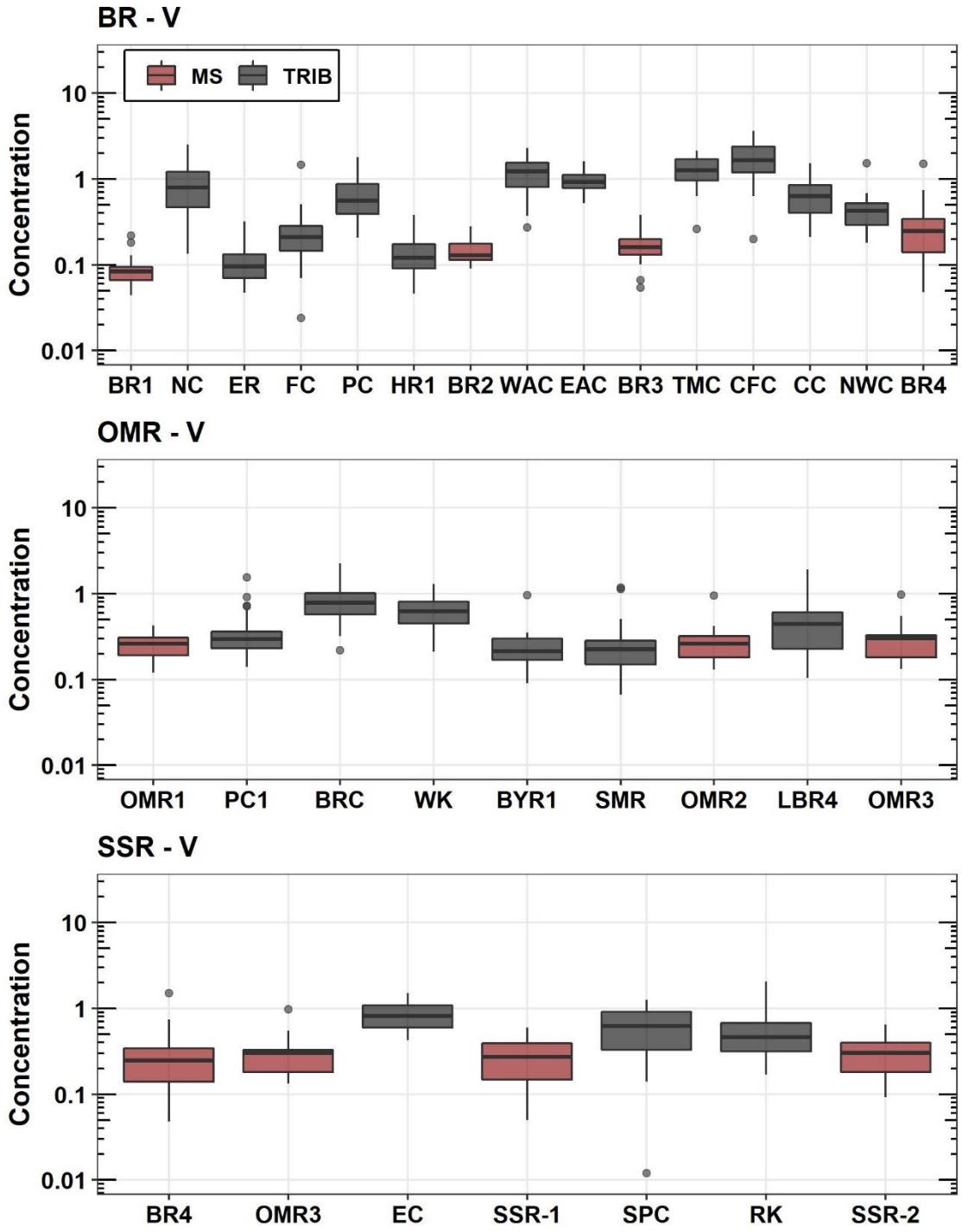

Figure S24: Box plots of the modelled dissolved Vanadium (V) concentrations for the Bow River (BR – Top), Oldman River (OMR – middle) and South Saskatchewan River (SSR) including main stem (MS – red)) and tributary (TRIB – grey) sites for all annual samples.

4